[redacted] RM A53I21

NACA RM A53I21

NACA

RESEARCH MEMORANDUM

WIND-TUNNEL INVESTIGATION OF A 45° SWEPTBACK WING HAVING A SYMMETRICAL ROOT AND A HIGHLY CAMBERED TIP, INCLUDING THE EFFECTS OF FENCES AND LATERAL CONTROLS

By Joseph W. Cleary and Lee E. Boddy

Ames Aeronautical Laboratory
Moffett Field, Calif.

NATIONAL ADVISORY COMMITTEE
FOR AERONAUTICS

WASHINGTON

November 20, 1953

[redacted]

NACA RM A53I21

NATIONAL ADVISORY COMMITTEE FOR AERONAUTICS

RESEARCH MEMORANDUM

WIND-TUNNEL INVESTIGATION OF A 45° SWEPTBACK WING HAVING A SYMMETRICAL ROOT AND A HIGHLY CAMBERED TIP, INCLUDING THE EFFECTS OF FENCES AND LATERAL CONTROLS

By Joseph W. Cleary and Lee E. Boddy

SUMMARY

A wind-tunnel investigation has been conducted at Mach numbers from 0.25 to 0.94 of a 45° sweptback wing having varying camber along the span. Two other wings, one having no camber and one having uniform camber, were also tested for comparison. Each wing had an aspect ratio of 5.515, a taper ratio of 0.532, and a thickness of 10 percent of the chord perpendicular to the sweep reference line. Numerous fence combinations, an aileron, and two types of spoilers were also tested on the wing with the varying camber. Measurements were made of the forces, moments, hinge moments, and wing-surface pressures for most of the configurations tested.

The results indicate that the effects of the spanwise flow of the boundary layer were so predominantly powerful that changing the camber along the span had only a secondary effect on the pitching-moment characteristics of the wing. When the outward flow of the boundary layer was restricted by fences, the pitching-moment characteristics of the wing were similar to what might be predicted from the theoretical loading on the wing and from the estimated maximum section lift coefficients, except for a mild unstable break at the stall. The lateral controls were effective throughout the Mach number range, although the aileron did not maintain its effectiveness as well as the spoiler. At high angles of attack, a fence at the inner end of the aileron improved the rolling-moment effectiveness and provided a more linear variation of rolling moment with aileron angle. The spoiler produced rolling moments that compared favorably with those of the aileron, but its effectiveness was not maintained at high angles of attack.

INTRODUCTION

Numerous experimental investigations have demonstrated that most sweptback wings of high aspect ratio suffer from a breakdown of the flow over the outer portion of the wing at the higher lift coefficients. This phenomenon is caused largely by two factors: (1) the induced loading due to angle of attack is greater on the outer portions, and (2) the outward flow of the boundary layer enables the inner portions to sustain a considerably higher lift coefficient. (See, e.g., ref. 1.) The undesirable result is usually severe longitudinal instability of the wing and deterioration of aileron effectiveness and hinge-moment characteristics.

The investigation reported herein consisted of a study of the characteristics of a wing designed to avoid the flow breakdown on the outer portion, the design method being similar to that used in the past for unswept wings. A moderate amount of washout was incorporated to reduce the loading on the tip sections and to produce a favorable loading at cruising lift coefficients. Also, the tip sections were highly cambered so that they might have a higher maximum lift coefficient than the symmetrical root sections. In order to reduce the deleterious effects of the outward flow of the boundary layer, a systematic series of fences was tested on the wing. The results are compared with those of two previously tested wings, one which was uncambered and untwisted, and one which had approximately uniform camber and twist. In addition, lateral-control characteristics are presented for three different types of controls on the subject wing. These consisted of a plain round-nose aileron, a continuous spoiler, and rotatable spoilers.

All of the tests reported herein were conducted in the Ames 16-foot high-speed wind tunnel.

NOTATION

The rolling-moment coefficients of the model are presented with respect to an axis coincident with the fuselage reference line. All other model coefficients are with respect to the wind axes with the origin at the quarter-chord point of the mean aerodynamic chord in the plane of symmetry. All coefficients of the lateral-control investigation are based on the deflection of a single control device.

Coefficients

C_D drag coefficient, $\frac{\text{drag}}{qS}$

C_h aileron hinge-moment coefficient, $\frac{\text{hinge moment}}{2M_aq}$

C_L lift coefficient, $\frac{\text{lift}}{qS}$

C_l rolling-moment coefficient, $\frac{\text{rolling moment}}{qSb}$

C_m pitching-moment coefficient referred to $0.25\bar{c}$, $\frac{\text{pitching moment}}{qS\bar{c}}$

c_l section lift coefficient, $\frac{\text{lift per foot of span}}{qc}$

c_{l_i} section ideal lift coefficient

c_m section pitching-moment coefficient referred to 0.25c, $\frac{\text{pitching moment per foot of span}}{qc^2}$

P pressure coefficient, $\frac{p_l - p}{q}$

Symbols

b wing span, ft

c wing chord parallel to plane of symmetry, ft

c' wing chord normal to sweep reference line, ft

$\bar{c}$ mean aerodynamic chord of wing $\frac{2}{S}\int_0^{b/2} c^2 dy$, ft

h spoiler height, ft

i incidence of the wing chord c, deg

[redacted]

l fuselage length, ft

M Mach number

M_a area moment of aileron behind hinge line about hinge axis, ft^3

p free-stream static pressure, lb/sq ft

p_l local static pressure, lb/sq ft

q free-stream dynamic pressure, $\frac{1}{2}\rho V^2$, lb/sq ft

r fuselage section radius, ft

R Reynolds number based on $\bar{c}$

S wing area, sq ft

V free-stream velocity, ft/sec

x chordwise distance from the wing leading edge or the nose of the fuselage, ft

y lateral distance measured perpendicular to the plane of symmetry, ft

α angle of attack of the fuselage reference line, deg

Δ incremental change in any of the coefficients

δ_a aileron deflection measured in a plane perpendicular to hinge line, positive deflections downward, deg

η span station, $\frac{y}{b/2}$

θ angle of rotatable spoilers with respect to c, positive when rotated counterclockwise on the left wing panel, deg

ρ free-stream mass density, slugs/cu ft

Effectiveness and Control Parameters

C_{h_α} rate of change of aileron hinge-moment coefficient with angle of attack for δ_a of 0°, per deg

[redacted]

The following effectiveness and control parameters are averages for aileron angles between ±5°:

C_{h_δ} rate of change of aileron hinge-moment coefficient with aileron deflection, per deg

C_{l_δ} rate of change of rolling-moment coefficient with aileron deflection, per deg

C_{m_δ} rate of change of pitching-moment coefficient with aileron deflection, per deg

MODEL AND APPARATUS

Model Geometry

Three wings differing only in camber and twist but having identical plan form were tested on the same body. (See fig. 1.) These were the wing designed for the present investigation, herein called varying-camber wing; one having no twist or camber, herein called uncambered wing; and one having a uniform camber and approximately uniform twist, herein called constant-camber wing. All pertinent geometric details for the three wings and the body may be ascertained from information given in figure 1(a). The uncambered wing and the constant-camber wing were constructed of solid aluminum alloy, while the varying-camber wing had a solid steel spar with tin-bismuth covering to facilitate the installation of four rows of pressure orifices. All three wings had about equal stiffness, the measured aeroelastic twist being about 2° at the higher Mach numbers and angles of attack.

The varying-camber wing was designed with methods similar to those used in the past to estimate the stalling characteristics of unswept wings, that is, control of the spanwise point of initial stall by proper relation between the section loading and maximum section lift coefficient. (See, e.g., ref. 2.) A moderate amount of washout was employed to reduce the loading on the tips at high lift coefficients and to produce a favorable spanwise variation of loading at cruising lift coefficients. This washout occurred over the inner half of the semispan (fig. 1(a)) to approximate that required for uniform section lift coefficient at moderate lift coefficients. The camber of the wing increased from zero at the root to a maximum at the midsemispan, and was constant from the midsemispan to the tip, the purpose being to increase the maximum lift coefficient of the tip sections over that of the root sections. The camber chosen was considered to be the maximum consistent with maintaining linear section lift curves. This combination of twist and camber variation produced the theoretical loading and estimated maximum section

lift coefficients shown on the right of figure 1(b). Similar data are shown for the two comparison wings. The loading curves were calculated using the method of reference 3, while the maximum section lift coefficients were estimated from a combination of two-dimensional and swept-wing data. The value for the uncambered section was estimated by inspection of the lift characteristics of the outer sections of several 45° sweptback, uncambered wings, and is about 50 percent higher than would be indicated by application of simple-sweep concepts to two-dimensional data. The variation of maximum lift with camber (and hence across the span of the varying-camber wing) was determined by applying simple-sweep concepts to two-dimensional data for a large number of cambered sections. Approximately this same variation with camber was indicated by inspection of the limited amount of data for highly cambered swept wings. Since it was expected that considerable interchange of boundary layer between the sections would be involved, no attempt was made to correct the estimated maximum section lift coefficients for variation of Reynolds number along the span. Note that if each section of the wings had the characteristics predicted in figure 1(b), the uncambered wing would stall initially nearest the tip, with a considerable margin between c_l and $c_{l_{max}}$ at the inner sections; the constant-camber wing would stall initially near the midsemispan with about equal margin near the root and tip; and the varying-camber wing would stall initially over the inner 70 percent of the semispan.

Provision was made for the installation of up to five fences on each wing panel to minimize the interchange of boundary layer between the sections of the wing. These fences were not intended to be optimum for any one wing or test condition, but were merely made large enough to restrain the main part of the boundary layer. The locations of the fences and of the pressure orifices are given in figure 1(c).

Lateral Controls

The varying-camber wing was equipped with an aileron and two types of spoilers as illustrated in figure 1(d). These lateral controls were located on the highly cambered part of the wing, the controls extending from 0.50 semispan to the wing tip. This and other pertinent dimensions of the controls can be obtained from figure 1(d). The aileron was of the plain round-nose type with the gap between the nose and the wing unsealed. The aileron was instrumented for measuring hinge moments with an electrical resistance-type strain gage.

The continuous spoiler was of constant-percent chord in height and was placed normal to the wing surface. The rotatable spoilers were equally spaced with their axes normal to the wing surface. Two sizes were used, the smaller size having one-fourth the area of the larger.

[redacted]

These spoilers were cambered with an $a = 1.0$ mean camber line for an ideal lift coefficient c_{l_i} of 1.0. They were positioned on the wing so that for 0° angle of attack the camber would produce a vortex generator effect opposing the outward flow of the boundary layer. (See fig. 1(d).)

Apparatus

The model was sting supported in the center of the Ames 16-foot high-speed wind tunnel as shown in figure 2. Normal force, axial force, pitching moment, and rolling moment of the model were measured by a strain-gage balance mounted within the fuselage. These forces and moments were resolved to give lift, drag, and pitching moment with respect to the wind axes and rolling moment about the fuselage center line. The angle of attack was measured with a pendulum-type, remotely indicating inclinometer mounted within the model. The pressure orifices were connected to a multiple-tube mercury manometer by means of flexible tubing.

TESTS

The tests were conducted at Mach numbers from 0.25 to 0.94 and at Reynolds numbers that varied from about 1.7×10^6 to 4.9×10^6. The average variation of Reynolds number with Mach number for these tests is shown in figure 3. At low Mach numbers the angle of attack was varied from about -1° to 24°; at the higher Mach numbers vibration, irregular motions of the model, and wind-tunnel-power limitations curtailed the angle-of-attack range. The tests consisted of measuring the normal force, axial force, pitching moment, and wing pressures for a systematic series of fence locations and fence combinations on the varying-camber wing. Also, normal force, axial force, and pitching moment were measured for the other two wings with two fences on each wing panel. The lateral-control tests consisted of normal-force, axial-force, pitching-moment, and rolling-moment measurements for various settings of the aileron and spoilers on the varying-camber wing. In addition, hinge moments and wing pressures were measured for various settings of the aileron.

Only a limited number of the data are presented in this report, particularly regarding the various fence combinations tested. However, the remainder are on file at the Ames Aeronautical Laboratory and may be obtained by request.

REDUCTION OF DATA

All force and moment data have been reduced to NACA standard dimensionless coefficients. Jet-boundary corrections were evaluated by the method of reference 4 and have been applied to the angle of attack and drag coefficient by adding the following:

$$\Delta\alpha = 0.43\ C_L \text{ deg}$$

$$\Delta C_D = 0.0076\ C_L^2$$

Blockage corrections have been applied to the Mach number calibration of the wind tunnel by the theoretical method of reference 5. This correction was of no practical significance for Mach numbers less than 0.80, but at the highest Mach number of the tests the corrected Mach number was 1.5 percent greater than the indicated Mach number. Measurements of the difference between the static pressure at the fuselage base and free-stream static pressure were used to correct the drag to that for free-stream static pressure at the base. No tare corrections have been applied to the coefficients for the effect of the sting support except for the base-pressure corrections to the drag. For tail-off models, the sting tares are believed to be small.

RESULTS AND DISCUSSION

Wing Characteristics

The lift, drag, and pitching-moment characteristics of the varying-camber wing are compared with those of the uncambered and the constant-camber wing in figure 4. Some data for the latter two wings (from both the present investigation and from previous tests in the Ames 12-foot pressure wind tunnel) have already been published in reference 6. Without fences (fig. 4(a)) all three wings showed severe longitudinal instability above moderate lift coefficients. In general, the varying-camber wing had no better pitching-moment characteristics than the constant-camber wing. The lift characteristics of the three wings were similar, with the two cambered wings having slightly higher maximum lifts. The drag characteristics of the varying-camber wing were slightly superior to those of the constant-camber wing below 0.2 lift coefficient and at all lift coefficients above 0.90 Mach number. However, this is believed to be due to excessive camber of the constant-camber wing and not to be a property of the varying camber.

Figure 4(b) compares the characteristics of the three wings having each wing panel fitted with the best combination of two fences, as

[redacted]

determined from the systematic series of fence combinations tested on the varying-camber wing. The pitching-moment characteristics of the uncambered wing were improved by the fences at moderate lift coefficients, but severe instability still existed at the stall. The characteristics of the two cambered wings were improved throughout the angle-of-attack range. As was the case without fences, the varying-camber wing showed little, if any, advantage over the constant-camber wing.

The characteristics of the varying-camber wing with a single fence and with five fences on each wing panel are presented in figure 5. The single fence shown was the most effective of the five fences tested and is also the configuration used later to restrict the boundary layer of the inner portion of the wing from flowing out over the aileron. With all five fences on each wing panel, the pitching-moment curves approached the desired linearity except for a mild unstable break at the stall. Note that the fences considerably reduced the drag of the model at the higher lift coefficient; whereas they caused a very small increase of drag at the low lift coefficients. (See figs. 4(a) and 5(b).)

Typical wing-pressure distributions with and without fences are shown in figure 6 for three angles of attack, one near the pitching-moment break (without fences), one near the stall, and one intermediate. At 0.25 Mach number, the innermost section, even with its small camber, maintained normal distribution with good pressure recovery up to the highest angle of attack; whereas the three outer sections without fences showed evidence of flow separation at angles of attack above the pitching-moment break. The fences enabled the two outer sections to maintain a more normal pressure distribution with considerably better recovery, while causing a reduction of the minimum-pressure peak of the inner section. The same trends are evident for 0.80 Mach number to a lesser degree.

The section lift and pitching-moment characteristics of the varying-camber wing, determined from integration of the pressure distributions, are shown in figure 7. Although data at more than four sections would be required to make a detailed analysis of the flow, in general, the fences greatly increased the lift-carrying capacity of the outer sections and slightly decreased the lift-carrying capacity of the inner sections. In fact, with all five fences and at 0.25 Mach number, the maximum section lift coefficient of the three outer sections agreed quite well with the predicted value shown in figure 1(b). However, the innermost section exceeded its predicted value by more than 50 percent. This accounts for the mild unstable break at the stall shown in figure 5(b).

The foregoing discussion indicates that the varying-camber wing without fences fell far short of having satisfactory pitching-moment characteristics. The outward flow of the boundary layer diminished

[redacted]

the lift-carrying capacity of the highly cambered tip sections, and increased the lift-carrying capacity of the symmetrical root sections to such an extent that the pitching-moment characteristics were hardly different from those of more conventional wings of similar plan form. When the outward flow of the boundary layer was restricted by means of fences, the sections of the outer two-thirds of the semispan had the expected lift characteristics, but the boundary-layer drain from the root was still sufficient to allow it to exceed its anticipated maximum lift by over 50 percent, causing a mild unstable moment at the stall. Thus, the pitching-moment curves were fairly linear up to the lift coefficient anticipated from examination of figure 1(b); however, the anticipated stable break at the stall was not realized.

Control Characteristics

An investigation of the lateral and longitudinal control characteristics of the model with the varying-camber wing was made with a plain aileron and two types of spoilers as control devices (see fig. 1(d)). The results are believed typical of the control characteristics of other rigid highly cambered wings of similar plan form. Since the aileron and spoilers both extended from 0.50 semispan to the wing tip, the results also serve as an indication of the relative merits of an aileron and spoiler for the particular conditions of the test. The aileron was mounted on the right wing panel and the spoilers were mounted on the left wing panel. Therefore, the rolling-moment coefficient due to a positive deflection of the aileron is normally of the same sign as that due to projecting the spoiler.

Plain aileron.- The rolling-moment, pitching-moment, and aileron hinge-moment characteristics of the model with and without a fence at 0.50 semispan are presented in figures 8, 9, and 10, respectively. These data are summarized in figure 11 to show the variation with Mach number of the effectiveness and hinge-moment parameters for angles of attack of 4.1° and 20.4°. These angles of attack were selected as representative of those at which a negligible amount of separation and extensive separation were observed. Although the data in figures 8, 9, and 10 are for selected Mach numbers, the curves in figure 11 have been prepared from data for several additional Mach numbers. Included in figure 11 is the low-speed value of the lateral-control effectiveness C_{l_δ} estimated by the use of reference 7. Close agreement between the estimate and experiment is indicated at low angles of attack and at 0.25 Mach number, the lowest Mach number of the tests.

From the results given in figures 8 and 9 it can be shown that as the angle of attack was increased above about 10° and the flow separation became more extensive, a gradual loss in control effectiveness

C_{l_δ} and C_{m_δ} occurred. This loss is illustrated in figure 11 by an approximately 50-percent decrease in C_{l_δ} and an even greater loss in C_{m_δ} between angles of attack of 4.1° and 20.4° at low Mach numbers for the model without the fence. However, due to the nonlinearity of the rolling- and pitching-moment curves of the model without the fence at the high angles of attack (figs. 8 and 9), the values given in figure 11 apply only for the limited range of aileron angles between ±5° for which C_{l_δ} and C_{m_δ} were evaluated.

The use of a fence at the midsemispan appeared to be of some advantage for improving the control characteristics at the high angles of attack. The fence generally increased the effectiveness and eliminated the highly nonlinear variation of rolling moment and pitching moment with aileron angle. However, the loss in effectiveness with increasing Mach number was quite similar with or without the fence. Between Mach numbers of 0.25 and 0.94 at low angles of attack, a decrease in C_{l_δ} of approximately 30 percent occurred (see fig. 11). Since a loss of only about 5 percent was estimated due to aeroelastic deformation of the wing, the predominant part of the total loss appears to have been of aerodynamic nature.

The variation of the hinge-moment parameters C_{h_α} and C_{h_δ} with Mach number shown in figure 11 illustrates that the effects of Mach number were small at low angles of attack. Although the fence increased C_{h_α} and C_{h_δ} at high angles of attack, a close similarity between the hinge-moment curves with and without the fence is shown in figure 10. In general, a smooth and approximately linear variation of hinge moment with aileron angle occurred at all Mach numbers from 0.25 to 0.94. Of interest is the relatively large floating angle of the aileron (about -10°) at low angles of attack. This was attributed primarily to the high camber of that part of the wing to which the aileron was attached.

Continuous spoiler.- Tests of a continuous constant-percent-chord spoiler were made to indicate the relative merits of the more common types of lateral controls. The results are presented in the rolling-moment, pitching-moment, and drag data of figures 12, 13, and 14, respectively, for several spoiler projections. These data have been cross-plotted against spoiler projection in figures 15, 16, and 17 to show some of the nonlinear characteristics of the spoiler. Of interest is the relatively high rolling effectiveness $d\Delta C_l/d(h/c)$ of the spoiler for projections less than 0.02c at angles of attack of 0° and 8° as compared with greater projections (see fig. 15). This relation is in contrast to the reduced, and in some cases reversed, effectiveness more commonly observed for small spoiler projections and may be the result of a "trigger" effect of the spoiler on the flow separation of this wing.

[redacted]

From figure 12 it is evident that the maximum rolling effectiveness of the spoilers was obtained at about 8° angle of attack and diminished with increasing angle of attack. This loss in effectiveness of the spoiler at high angles of attack may possibly be alleviated somewhat by using a plug spoiler as was done in reference 8 or a spoiler-deflector-slot combination as in reference 9.

While the spoiler compared unfavorably with the aileron at high angles of attack, it appeared to retain its effectiveness to a greater extent than the aileron at the high Mach number. This can be illustrated in the following way. At 4.1° angle of attack the aileron angle had to be increased 8° (11° to 19°) as the Mach number varied from 0.25 to 0.94 to match the rolling moment produced by a fixed spoiler projection of 0.05c. Projecting the spoiler generally increased the pitching moment and drag at all Mach numbers as shown in figures 16 and 17.

Rotatable spoilers.- A step-type rotatable spoiler was devised to investigate the possibility of improving spoiler rolling effectiveness at the higher angles of attack through the use of a nonretractable-type lateral control. It was thought that this might be accomplished if the spoilers were set at such an angle that they would act as vortex generators and would reduce the flow separation, thus increasing the lift and producing rolling moment opposite to that of conventional spoilers. Differential linking of left and right spoilers might, therefore, extend the rolling effectiveness to higher angles of attack. The results are indicated by the rolling-moment, pitching-moment, and drag data in figures 18, 19, and 20, respectively. As can be seen from figure 18, the spoilers were most effective as vortex generators for settings of 22.5° and 45°. For these settings, positive increments of rolling moment due to the spoiler were obtained for angles of attack between about 8° and 14°. Other spoiler angles generally decreased the lift and caused negative rolling moments. Thus, for this particular wing, the usefulness of this type of spoiler appears limited to developing additional rolling moment at intermediate angles of attack with no appreciable improvement at high angles of attack.

The use of spoilers as a nonretractable lateral control would be governed to some extent by the amount of increased drag that would be acceptable. The least increase in drag occurred for the 0° and 22.5° spoiler angles.

CONCLUDING REMARKS

The results of tests of a 45° sweptback wing having increasing camber along the span (intended to prevent tip stall) indicate that the

effects of the spanwise flow of the boundary layer are so predominantly powerful that changing the camber along the span had a secondary effect on the pitching-moment characteristics of the wing. When the outward flow of the boundary layer was restricted by fences, the moment characteristics of the wing were similar to what might be predicted from the theoretical loading on the wing and the estimated maximum section lift coefficients, except for a mild unstable break at the stall.

The results of tests of lateral-control devices on the wing indicate that control effectiveness was generally maintained for Mach numbers from 0.25 to 0.94. At high angles of attack, fences at the mid-semispan (the inner end of the aileron) improved the rolling-moment effectiveness and provided a more linear variation of rolling moment with aileron angle. The spoiler produced rolling moments that compared favorably with those of the aileron, but its effectiveness was not maintained at high angles of attack.

Ames Aeronautical Laboratory
National Advisory Committee for Aeronautics
Moffett Field, Calif., Sept. 21, 1953

REFERENCES

1. Hunton, Lynn W.: Effects of Finite Span on the Section Characteristics of Two 45° Sweptback Wings of Aspect Ratio 6. NACA TN 3008, 1953.

2. Anderson, Raymond F.: A Comparison of Several Tapered Wings Designed to Avoid Tip Stalling. NACA TN 713, 1939.

3. DeYoung, John, and Harper, Charles W.: Theoretical Symmetric Span Loading at Subsonic Speeds for Wings Having Arbitrary Plan Form. NACA Rep. 921, 1948.

4. Silverstein, Abe, and White, James A.: Wind-Tunnel Interference With Particular Reference to Off-Center Positions of the Wing and to the Downwash at the Tail. NACA Rep. 547, 1935.

5. Herriot, John G.: Blockage Corrections for Three-Dimensional-Flow Closed-Throat Wind Tunnels, With Consideration of the Effect of Compressibility. NACA Rep. 995, 1950. (Supersedes NACA RM A7B28.)

6. Shibata, Harry H., Bandettini, Angelo, and Cleary, Joseph W.: An Investigation Throughout the Subsonic Speed Range of a Full-Span and a Semispan Model of a Plane Wing and of a Cambered and Twisted Wing, All Having 45° Sweepback. NACA RM A52D01, 1952.

[redacted]

7. Lowry, John G., and Schneiter, Leslie E.: Estimation of Effectiveness of Flap-Type Controls on Sweptback Wings. NACA TN 1674, 1948.

8. Hammond, Alexander D., and Watson, James M.: Lateral-Control Investigation at Transonic Speeds of Retractable Spoiler and Plug-Type Spoiler-Slot Ailerons on a Tapered 60° Sweptback Wing of Aspect Ratio 2. Transonic-Bump Method. NACA RM L52F16, 1952.

9. Watson, James M.: Low-Speed Lateral-Control Investigation of a Flap-Type Spoiler Aileron With and Without a Deflector and Slot on a 6-Percent-Thick, Tapered, 45° Sweptback Wing of Aspect Ratio 4. NACA RM L52G10, 1952.

[redacted]

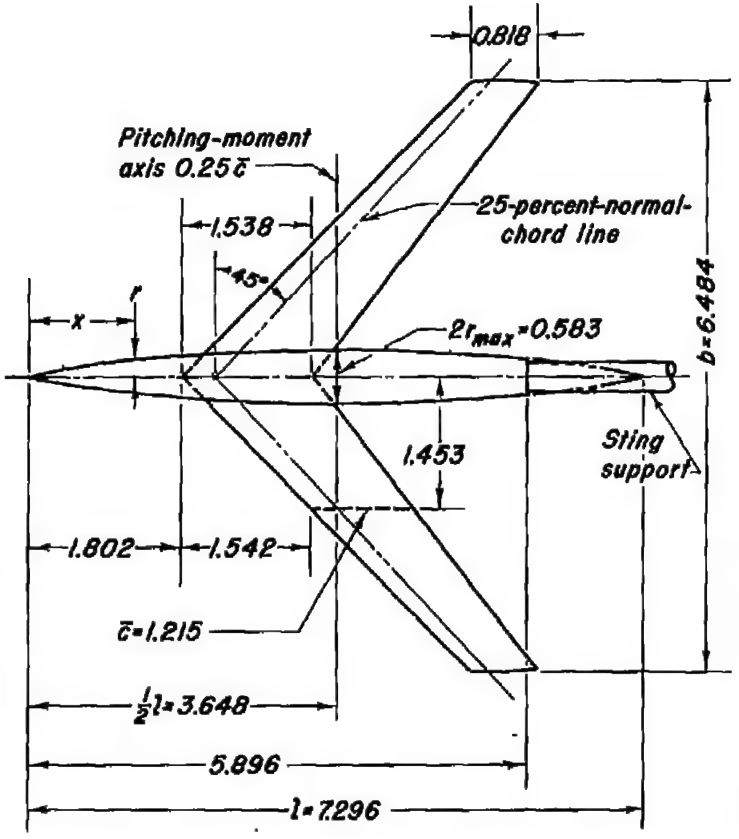

Note: All dimensions in feet unless otherwise specified.

Equation of fuselage ordinates $\frac{r}{r_{max}}=\left[1-\left(1-\frac{2x}{l}\right)^2\right]^{\frac{3}{4}}$

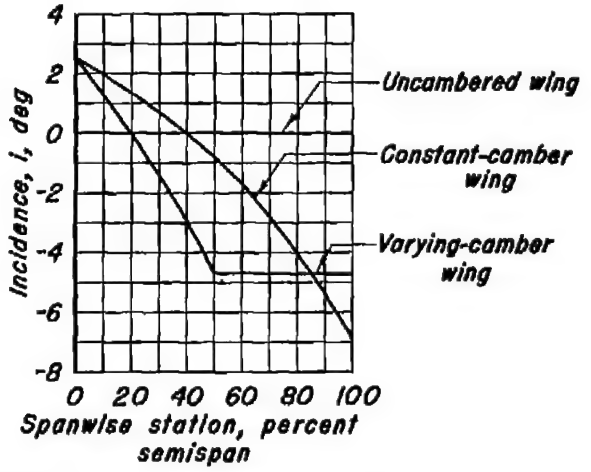

Incidence of the geometric chord.

Wing Geometry				
		Wing		
		Uncambered	Constant camber	Varying camber
Aspect ratio		5.515	5.515	5.515
Taper ratio		0.532	0.532	0.532
Dihedral, degree		0	0	0
*Airfoil section	Root	NACA64A010	NACA64A810	NACA64A010
	Midsemispan	NACA64A010	NACA64A810	NACA64A610
	Tip	NACA64A010	NACA64A810	NACA64A610

NACA

*Sections perpendicular to 25-percent-chord line. Mean line a = 0.8 (modified).

(a) Plan form and section details of the model with the three wings.

Figure 1.- Geometric and design details of the model.

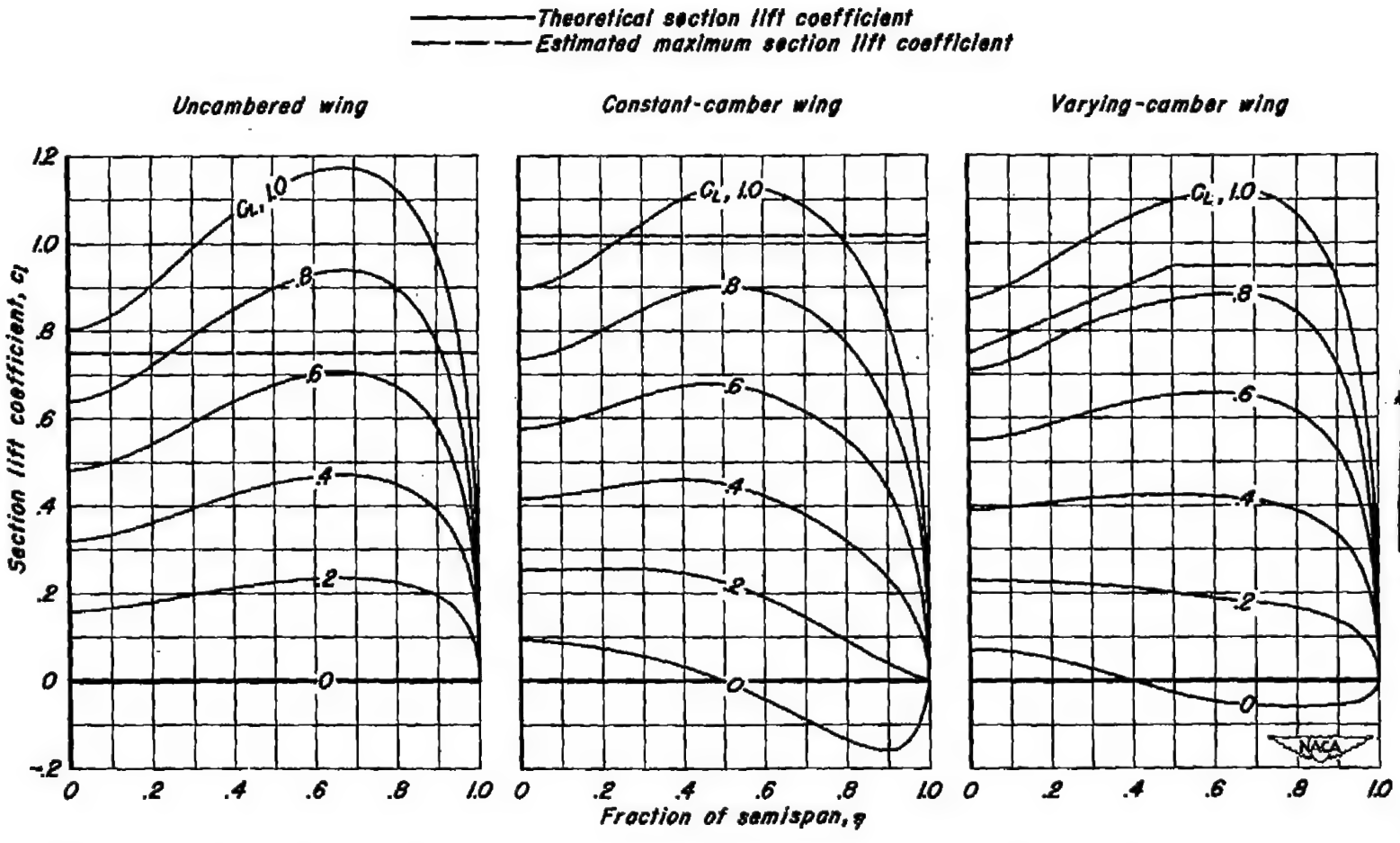

(b) Estimated spanwise variation of section lift coefficient and maximum section lift coefficient for the three wings.

Figure 1.–Continued.

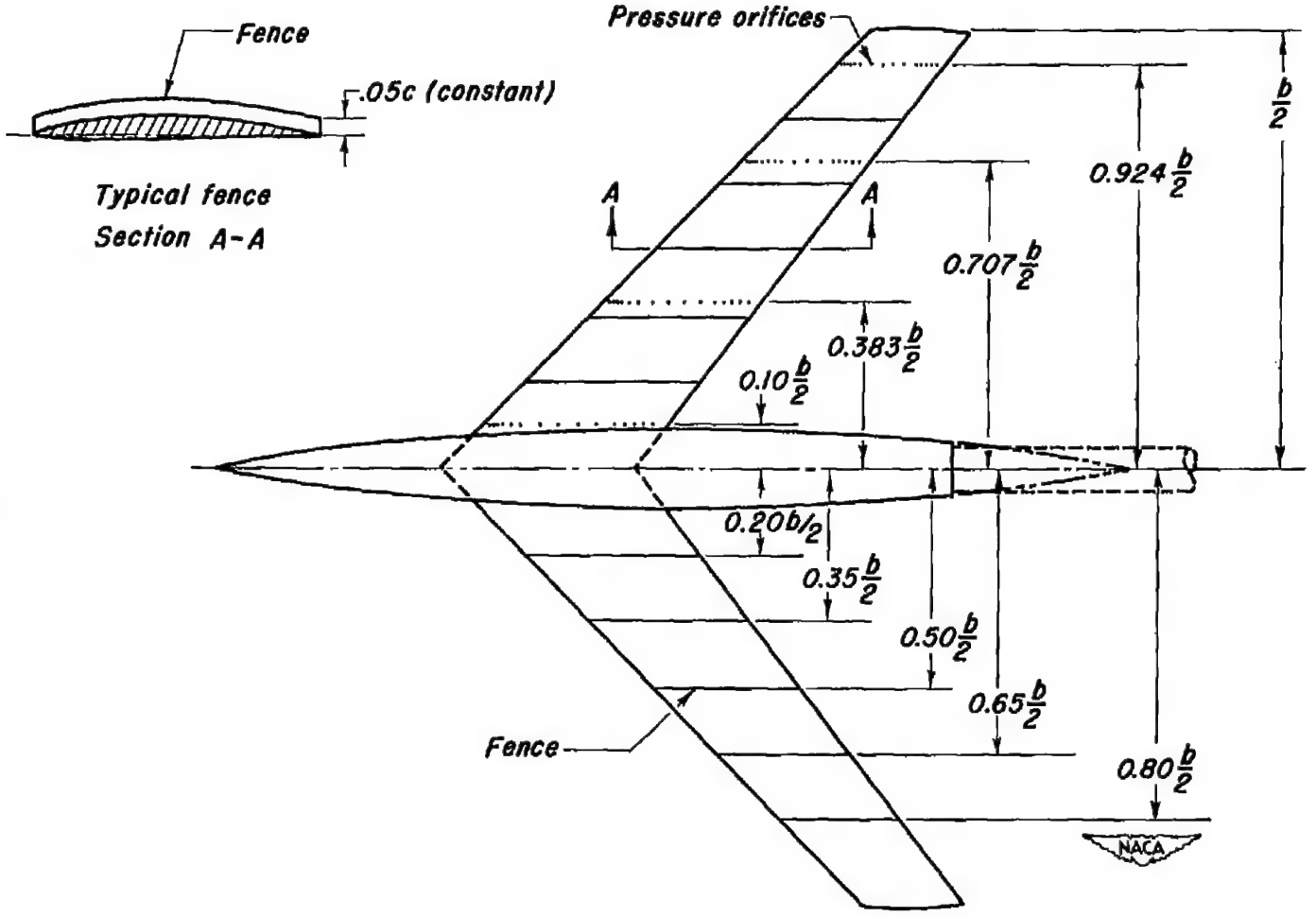

(c) Fences and pressure orifice locations on the varying-camber wing.

Figure 1.—Continued.

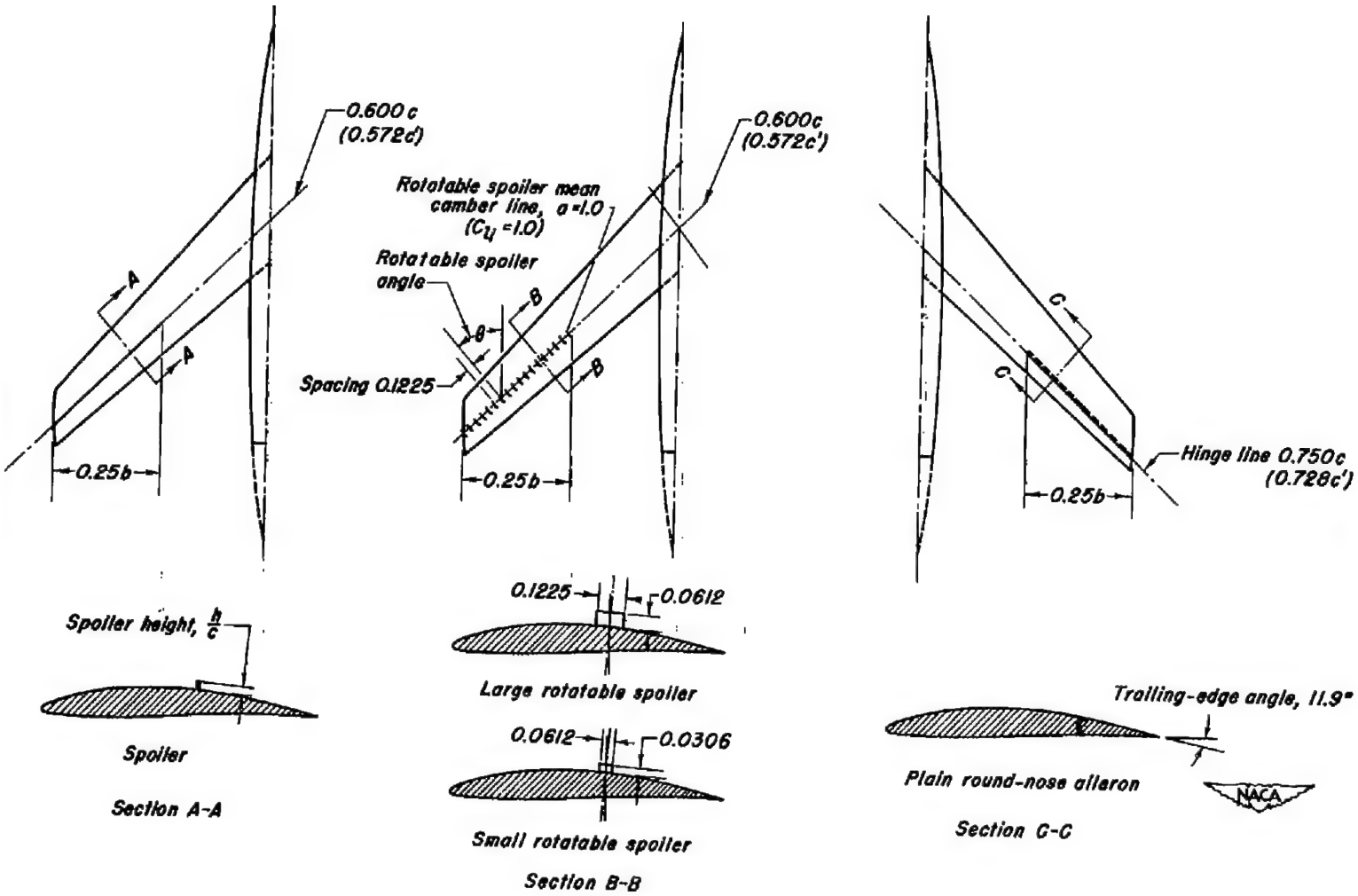

Note: All dimensions in feet unless otherwise specified.

(d) Lateral-control devices on the varying-camber wing.

Figure 1.- Concluded.

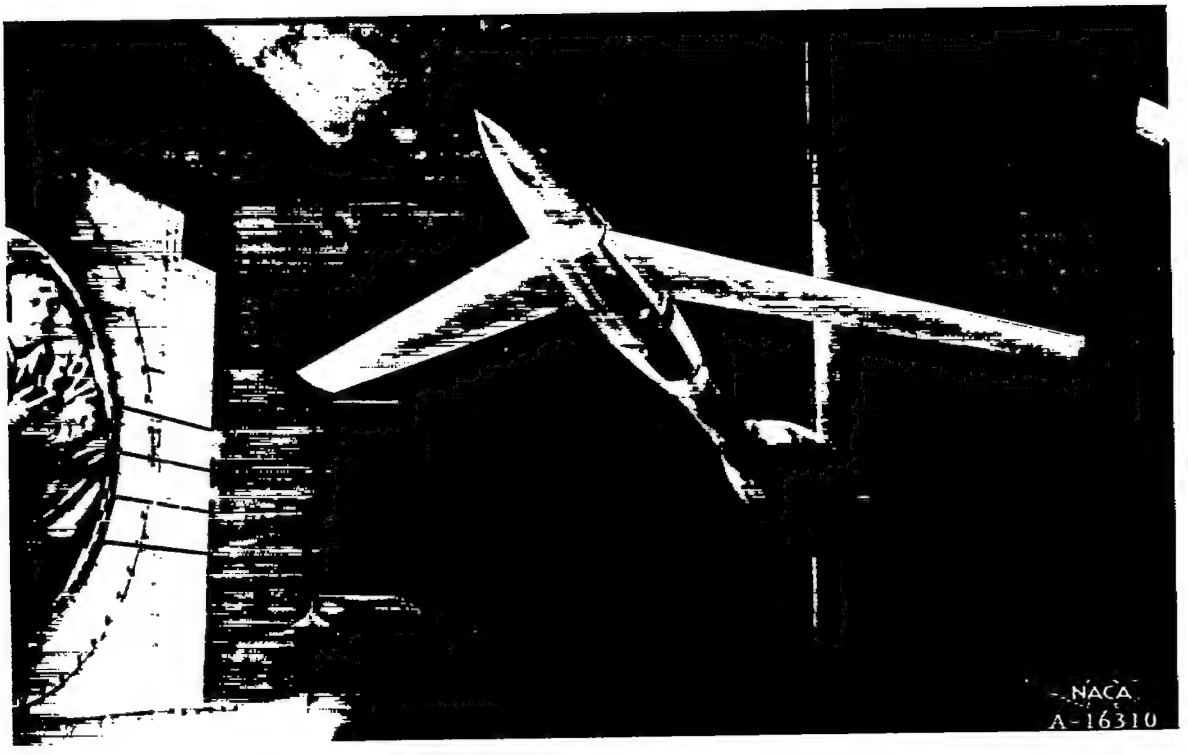

Figure 2.- Photograph of the model supported in the Ames 16-foot high-speed wind tunnel.

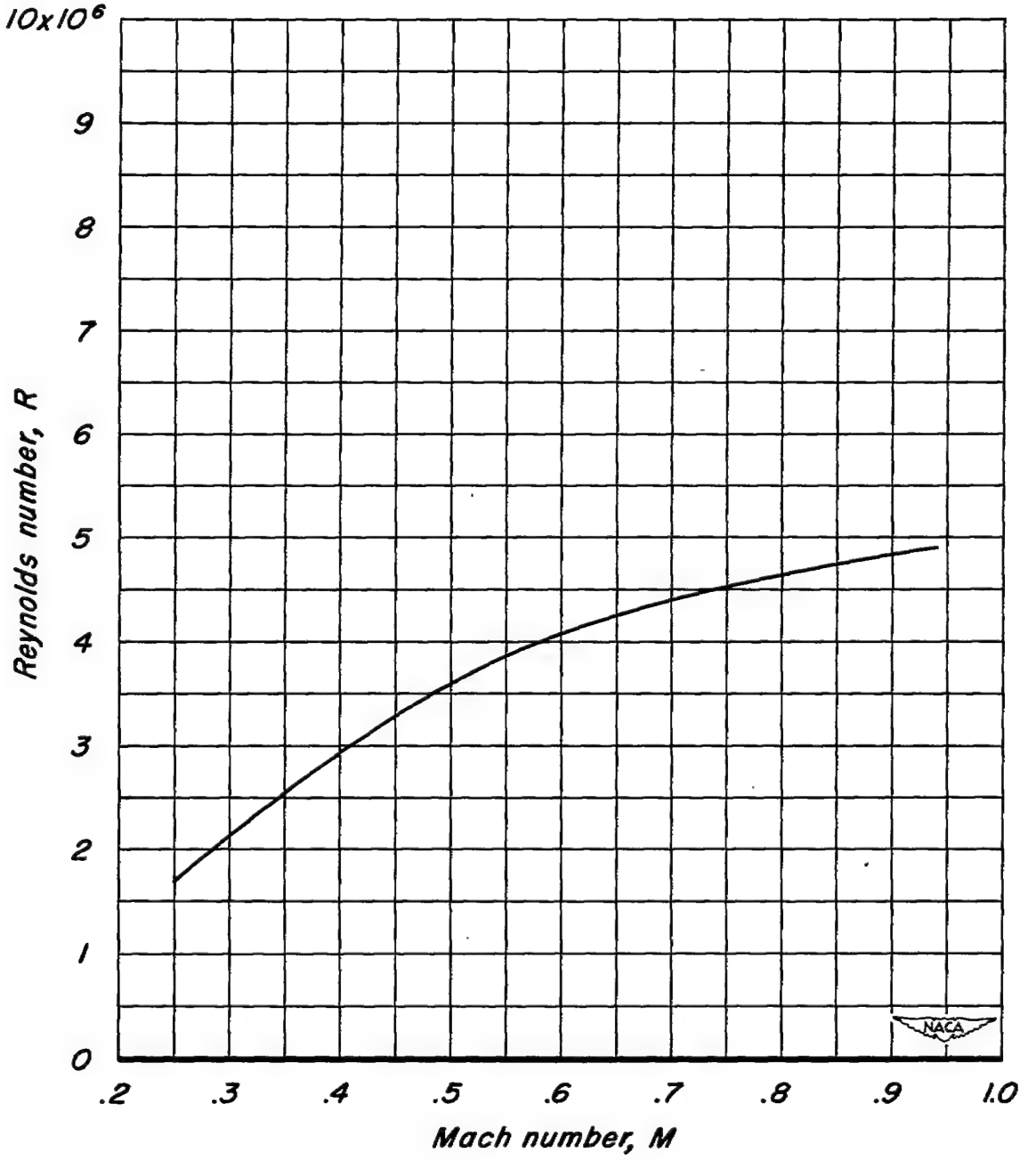

Figure 3.- The variation of Reynolds number with Mach number.

[redacted]

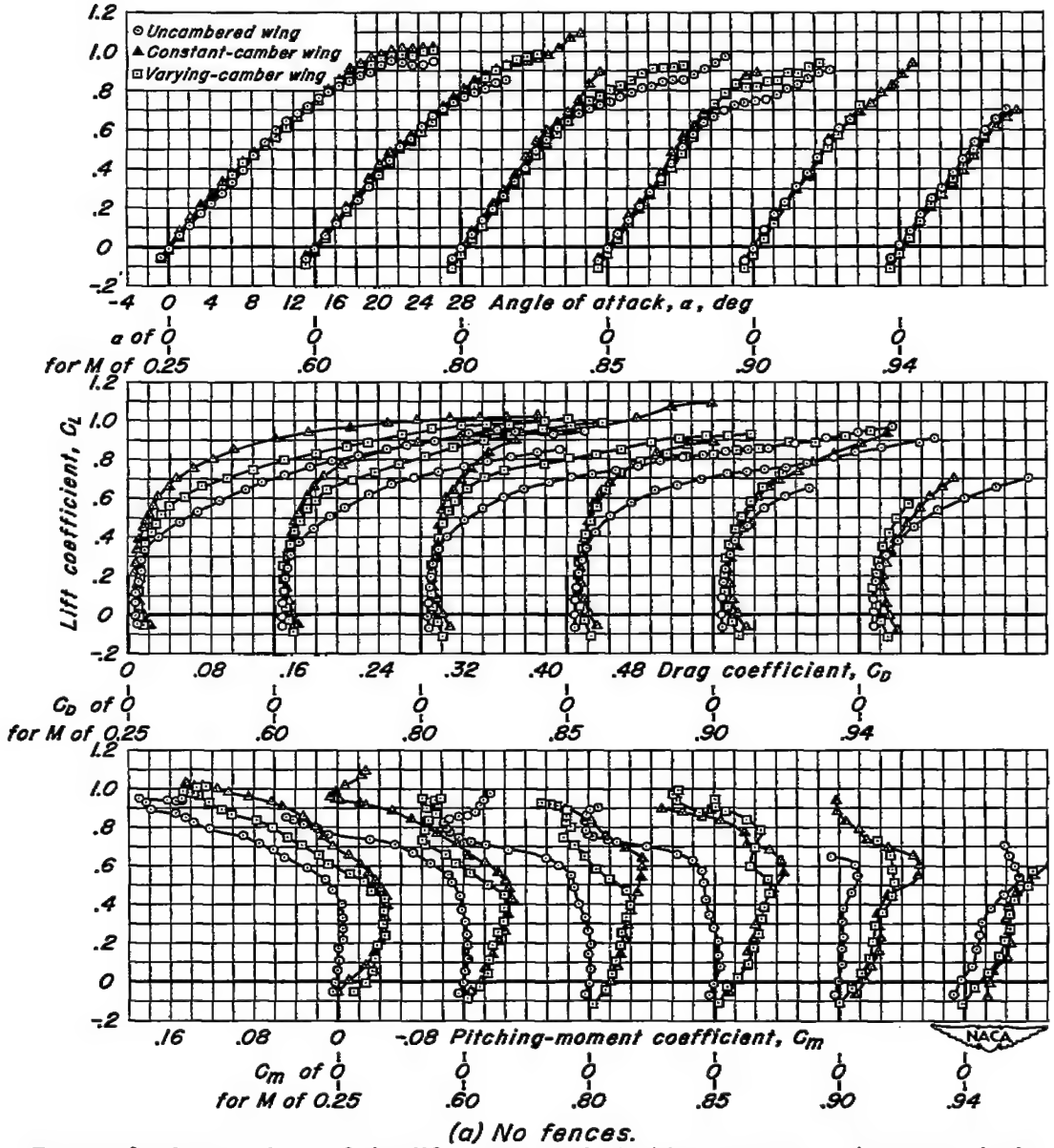

(a) No fences.

Figure 4.- Comparison of the lift, drag, and pitching-moment characteristics of the model with the three different wings.

[redacted]

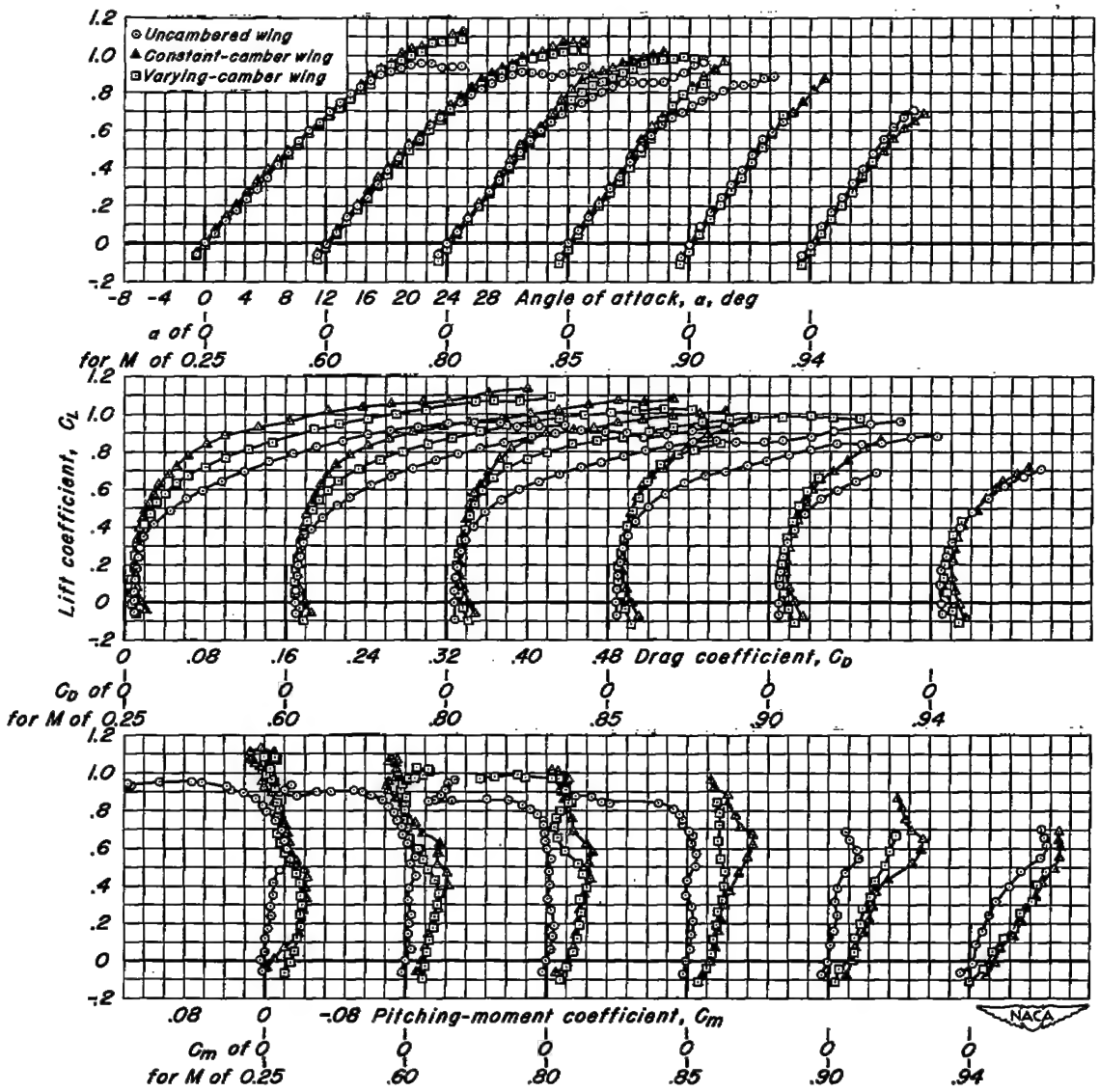

(b) Fences at η of 0.50 and 0.65.

Figure 4.- Concluded.

[redacted]

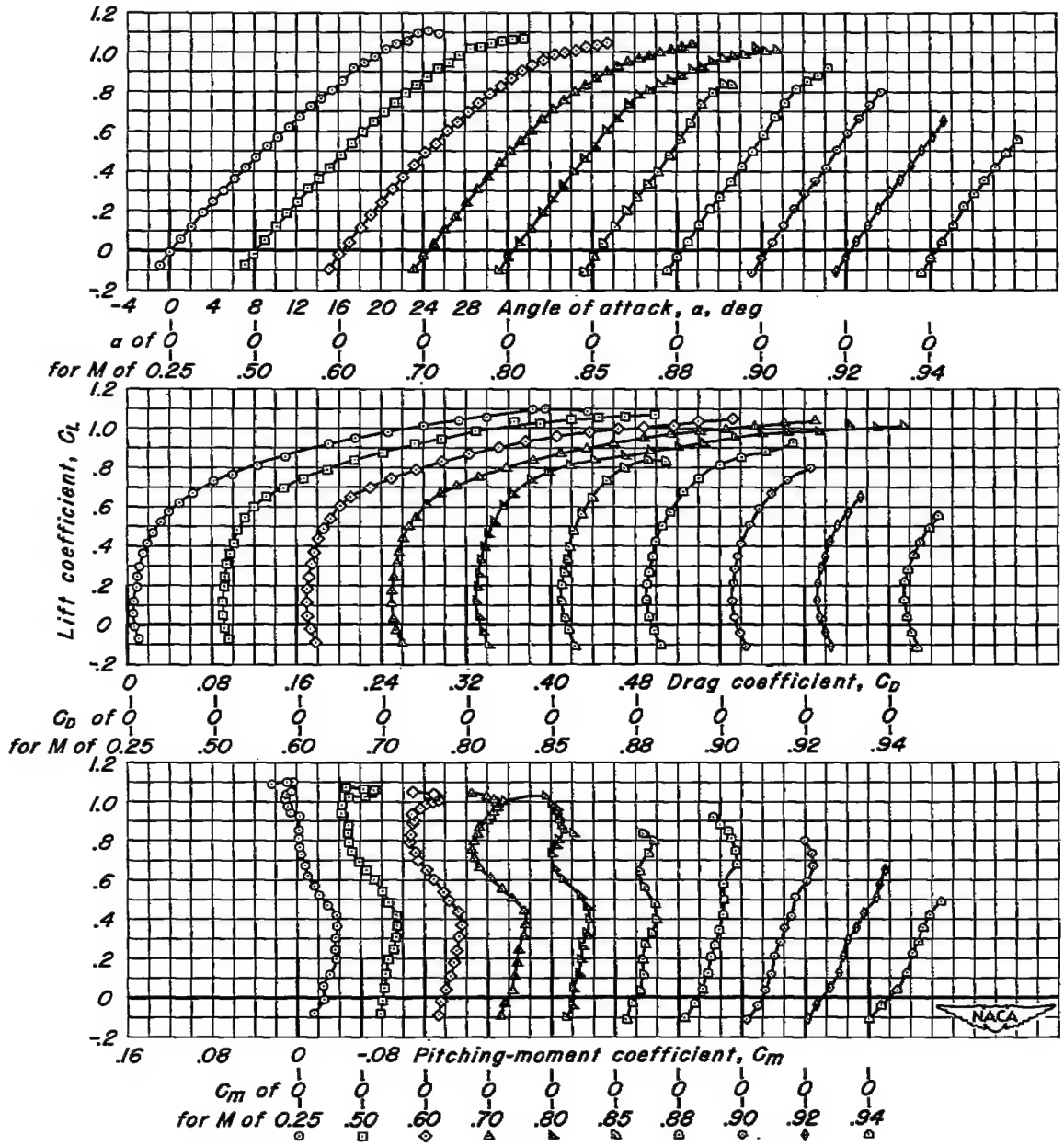

(a) Fence at η of 0.50.

Figure 5.—The lift, drag, and pitching-moment characteristics of the model with the varying-camber wing with two different combinations of fences.

[redacted]

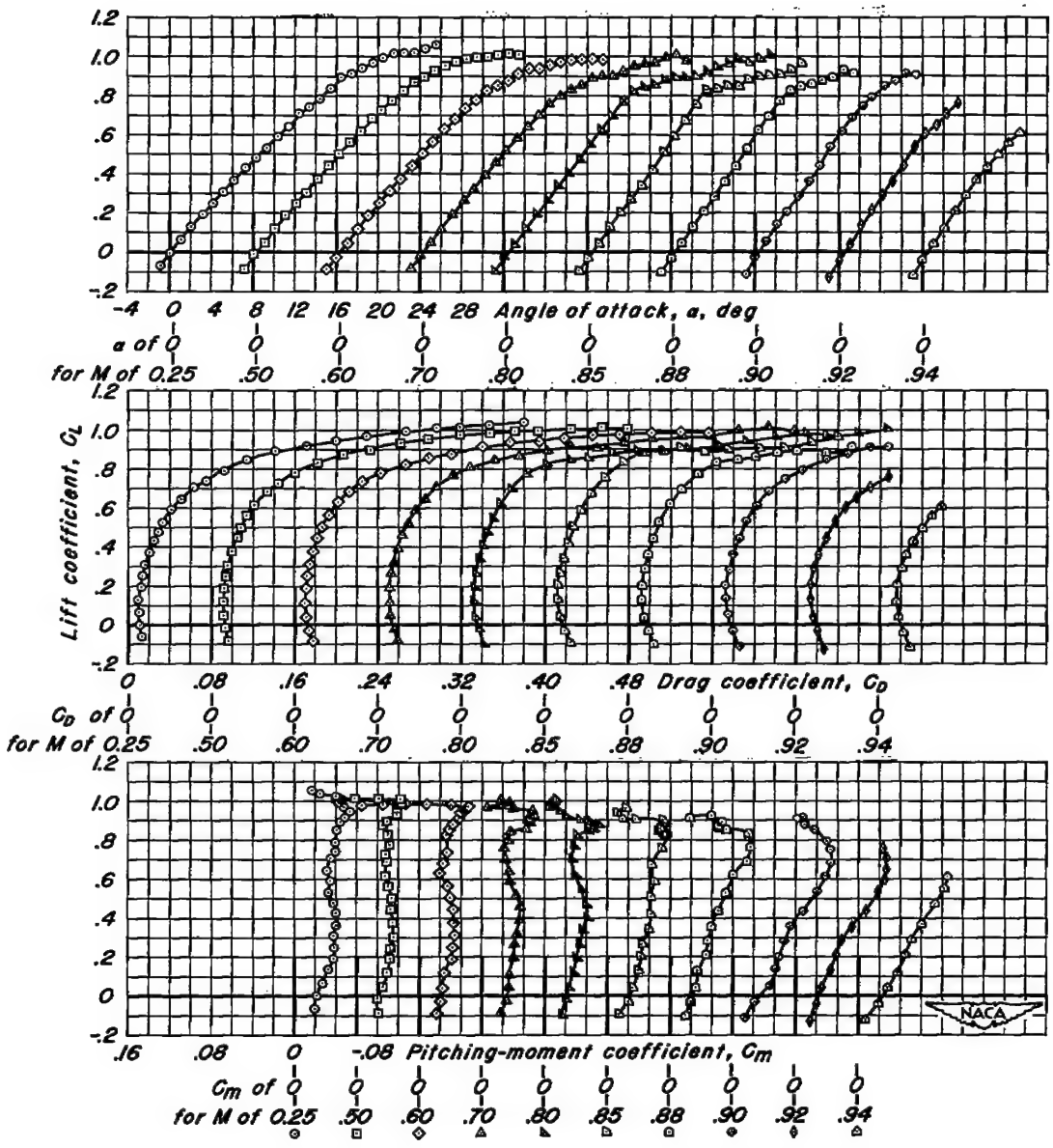

(b) Fences at η of 0.20, 0.35, 0.50, 0.65, and 0.80.

Figure 5.- Concluded.

[redacted]

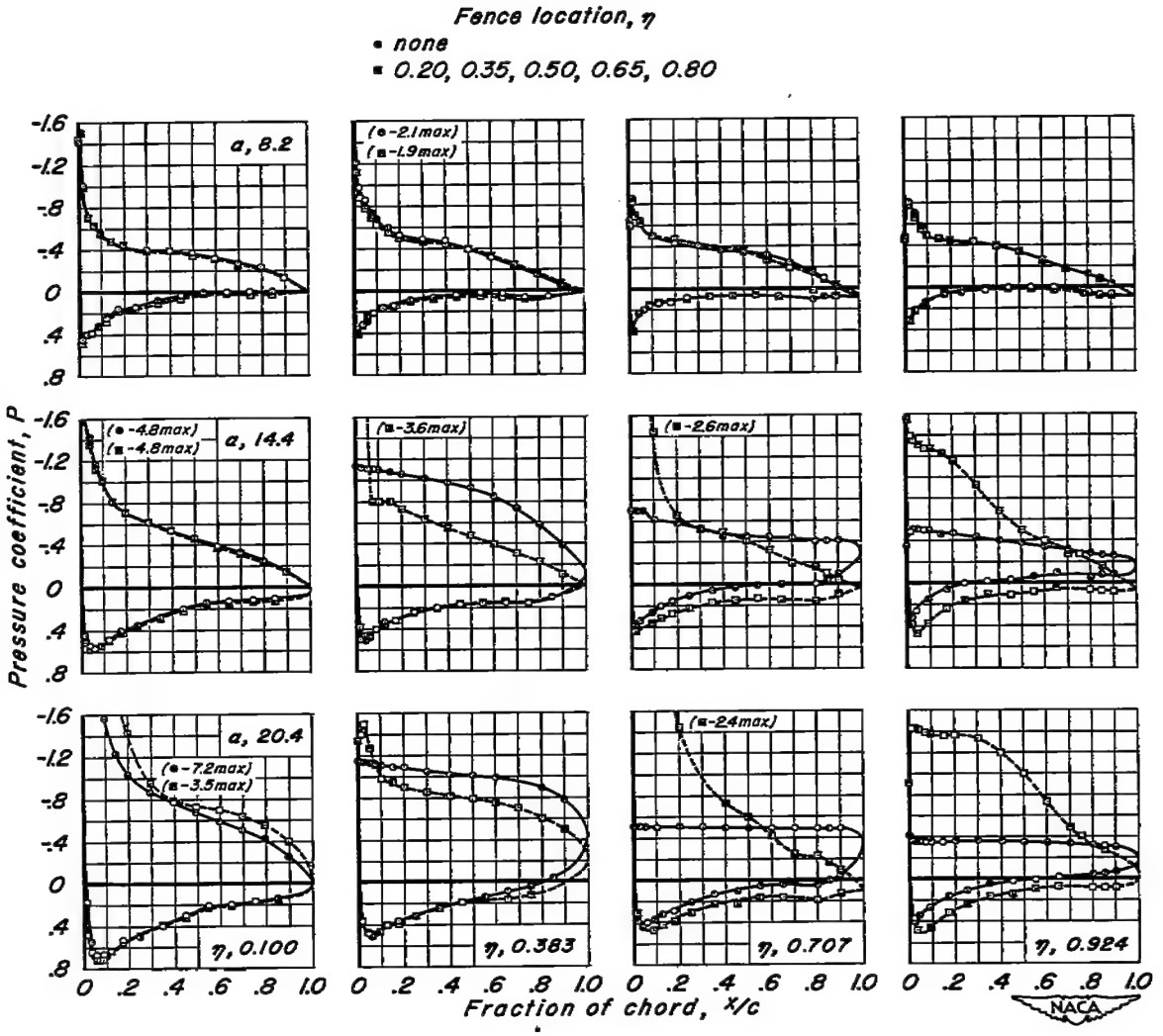

(a) Mach number of 0.25.

Figure 6.—The effect of fences on the chordwise pressure distribution at four spanwise stations of the varying-camber wing.

[redacted]

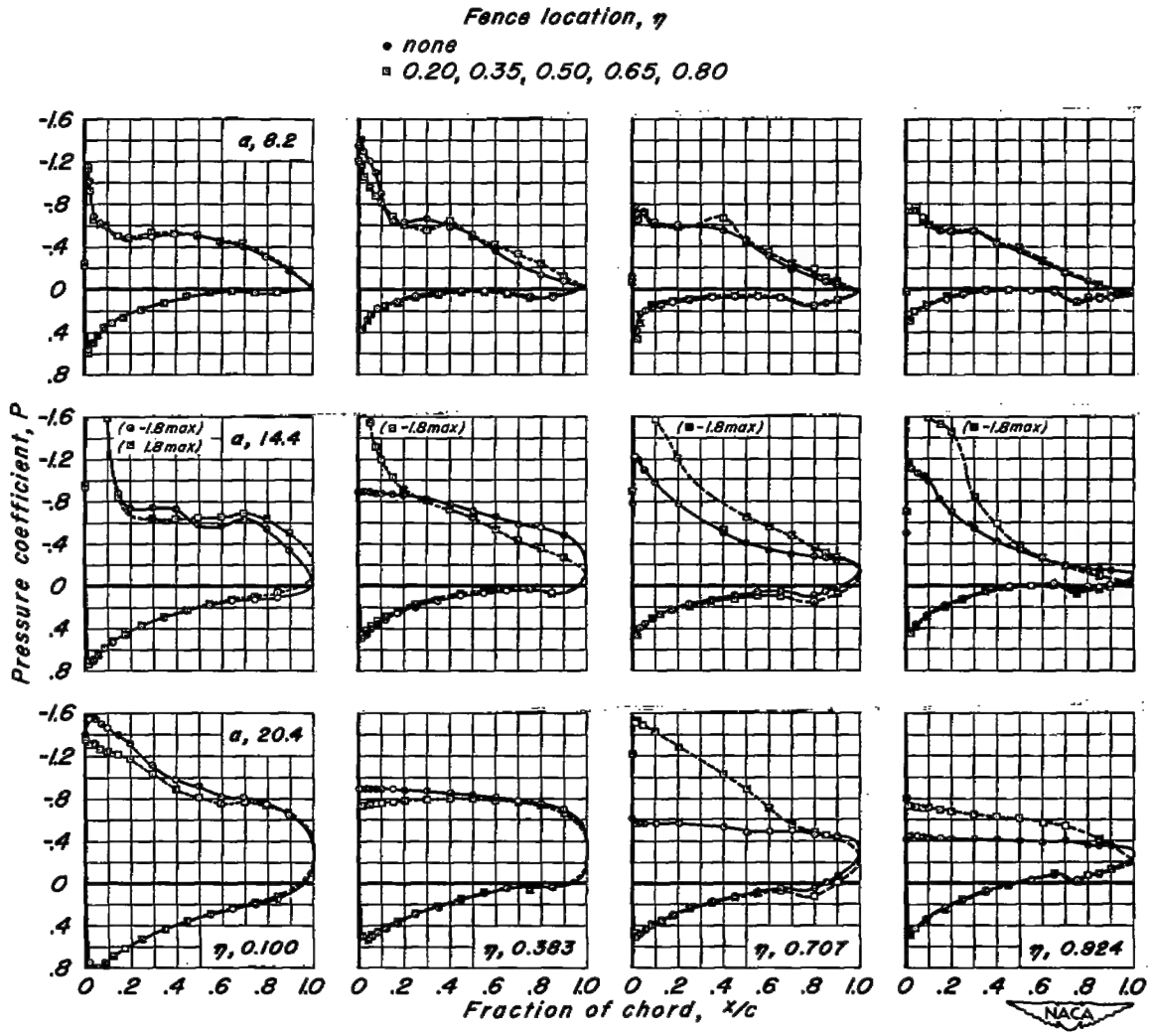

(b) Mach number of 0.80.

Figure 6.–Concluded.

[redacted]

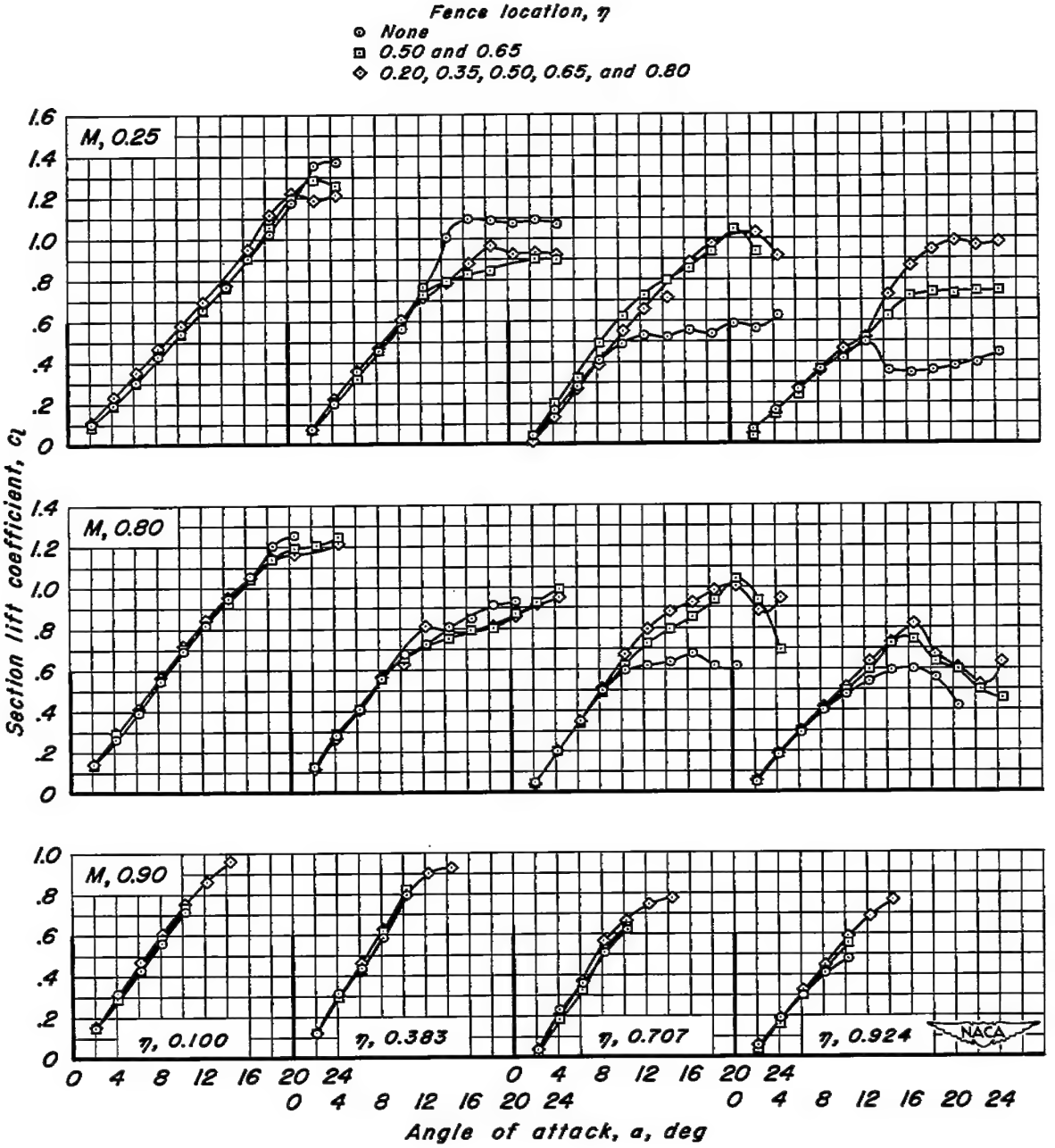

(a) Section lift coefficient.

Figure 7.–The effect of different combinations of fences on the section lift and pitching-moment characteristics of four sections of the varying-camber wing.

[redacted]

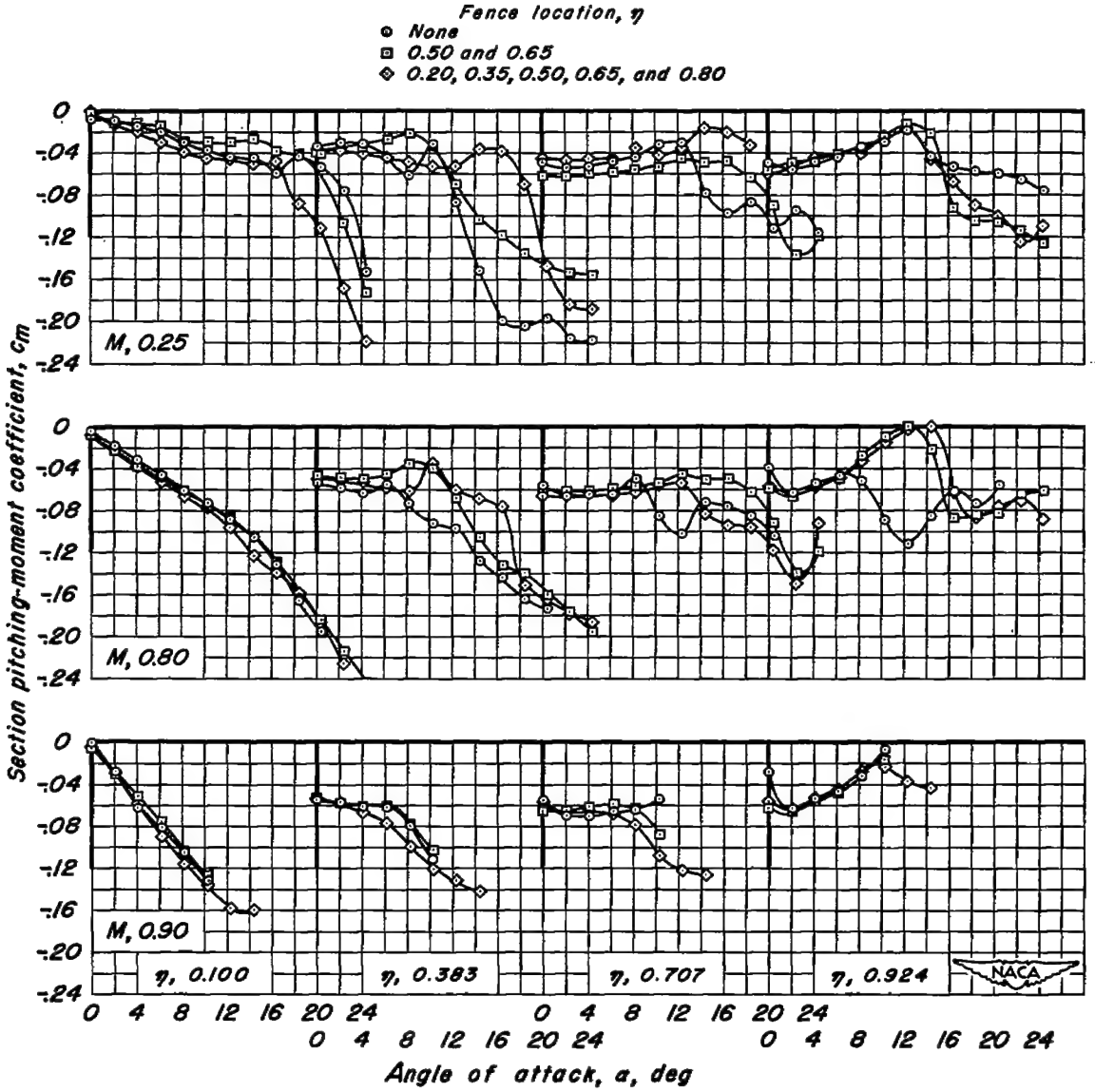

(b) Section pitching-moment coefficient.

Figure 7.–Concluded.

[redacted]

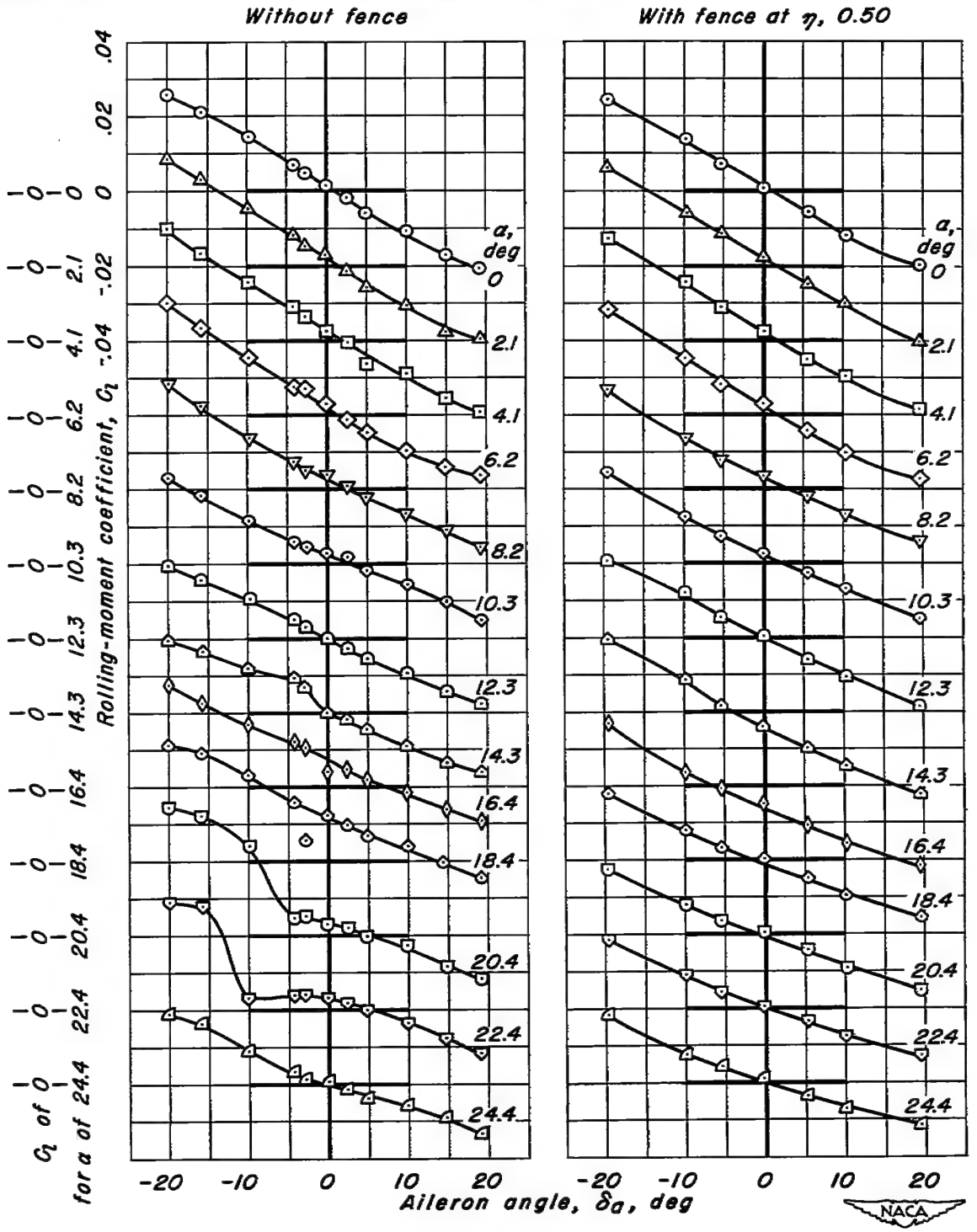

(a) M, 0.25

Figure 8.–The variation of rolling-moment coefficient with aileron angle.

[redacted]

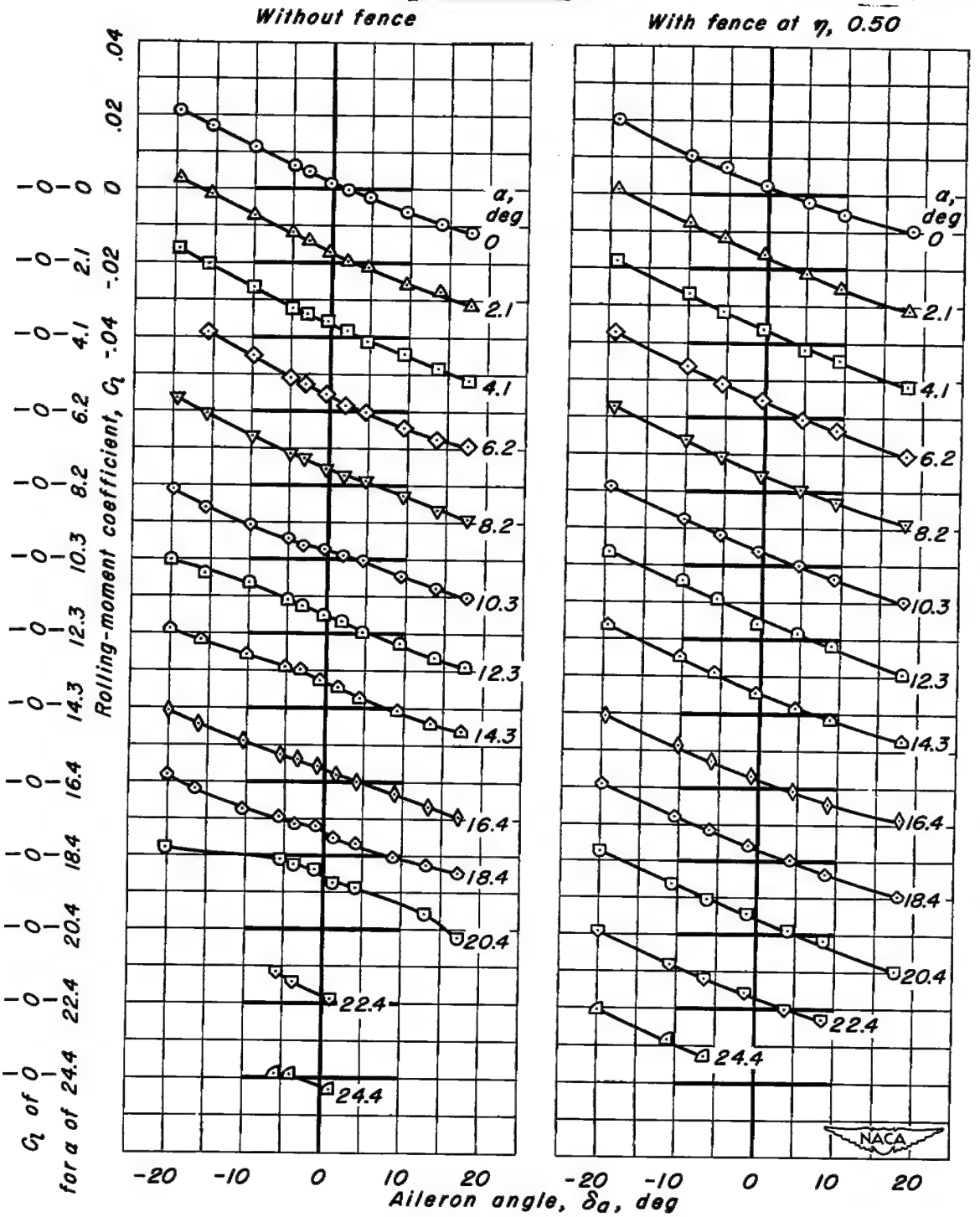

(b) M, 0.80

Figure 8.—Continued.

[redacted]

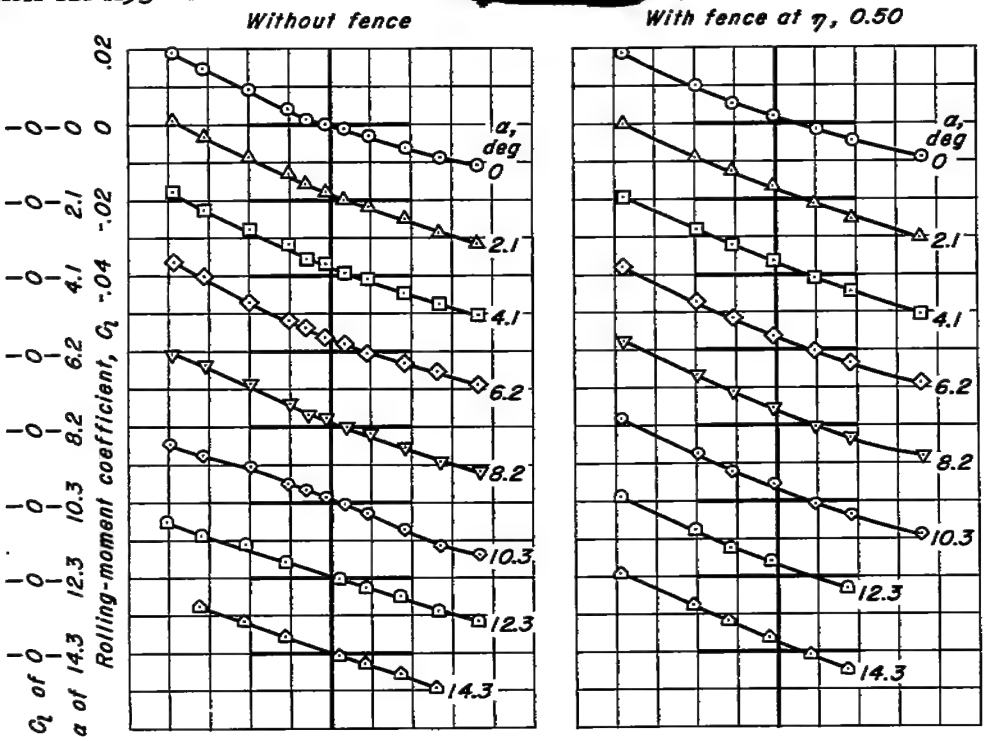

(c) M, 0.90

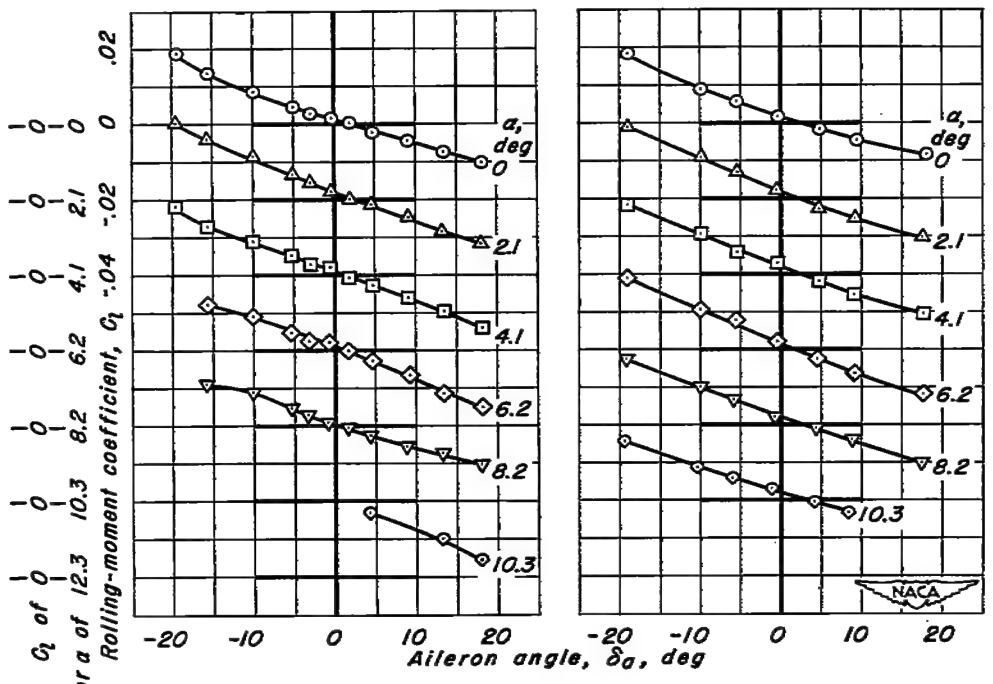

(d) M, 0.94

Figure 8.—Concluded

[redacted]

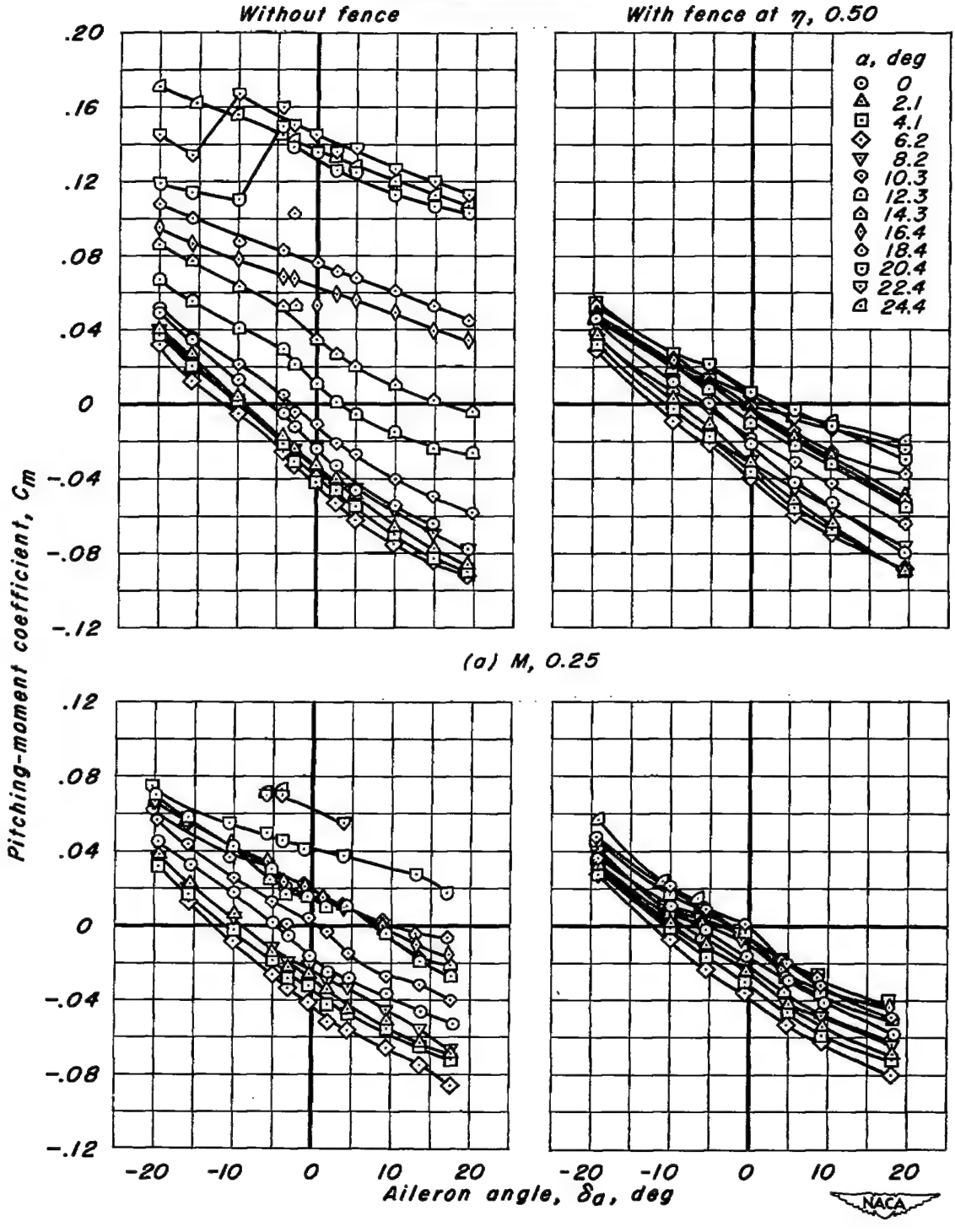

Figure 9.-The variation of pitching-moment coefficient with aileron angle.

[redacted]

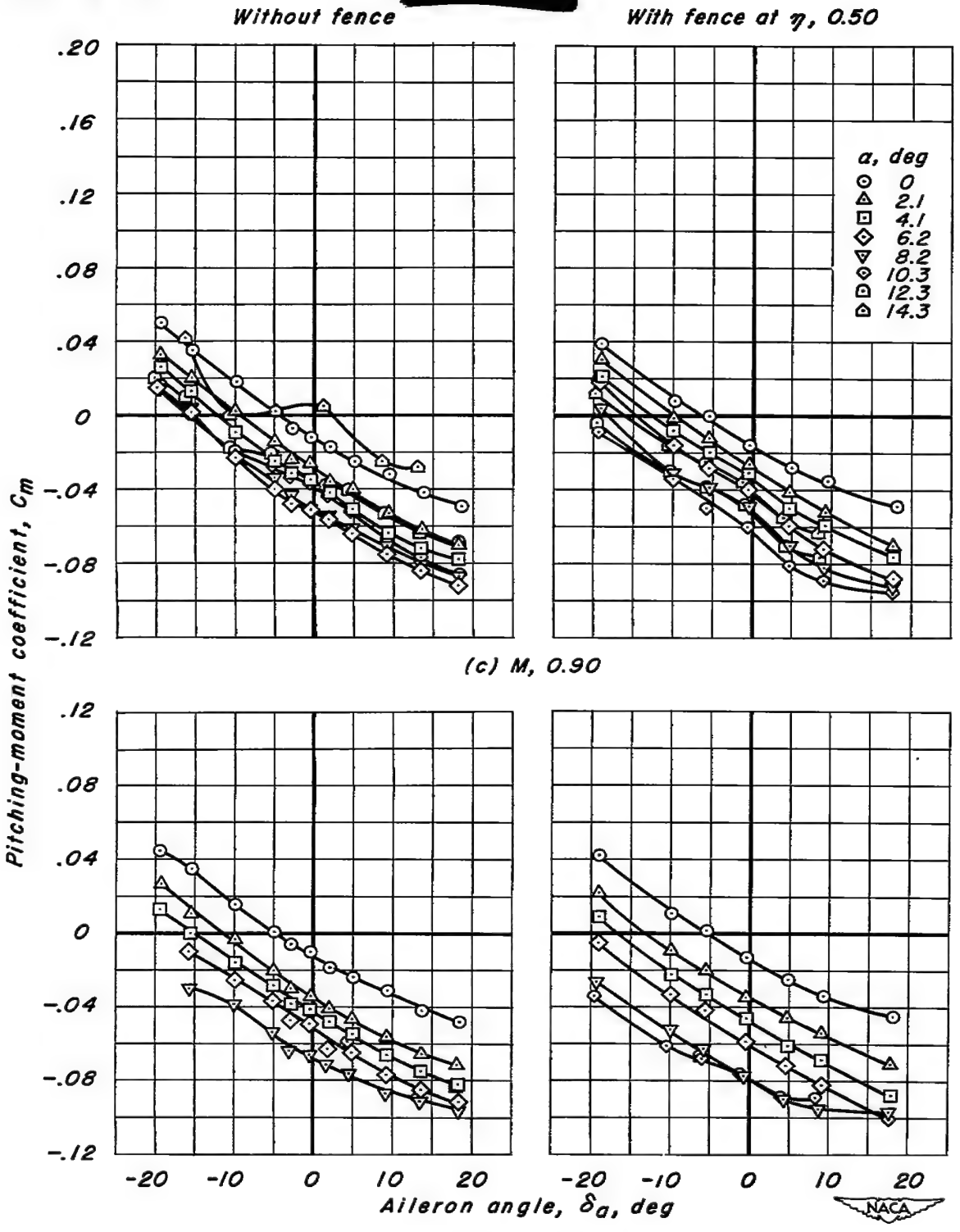

(c) M, 0.90

(d) M, 0.94

Figure 9.—Concluded.

[redacted]

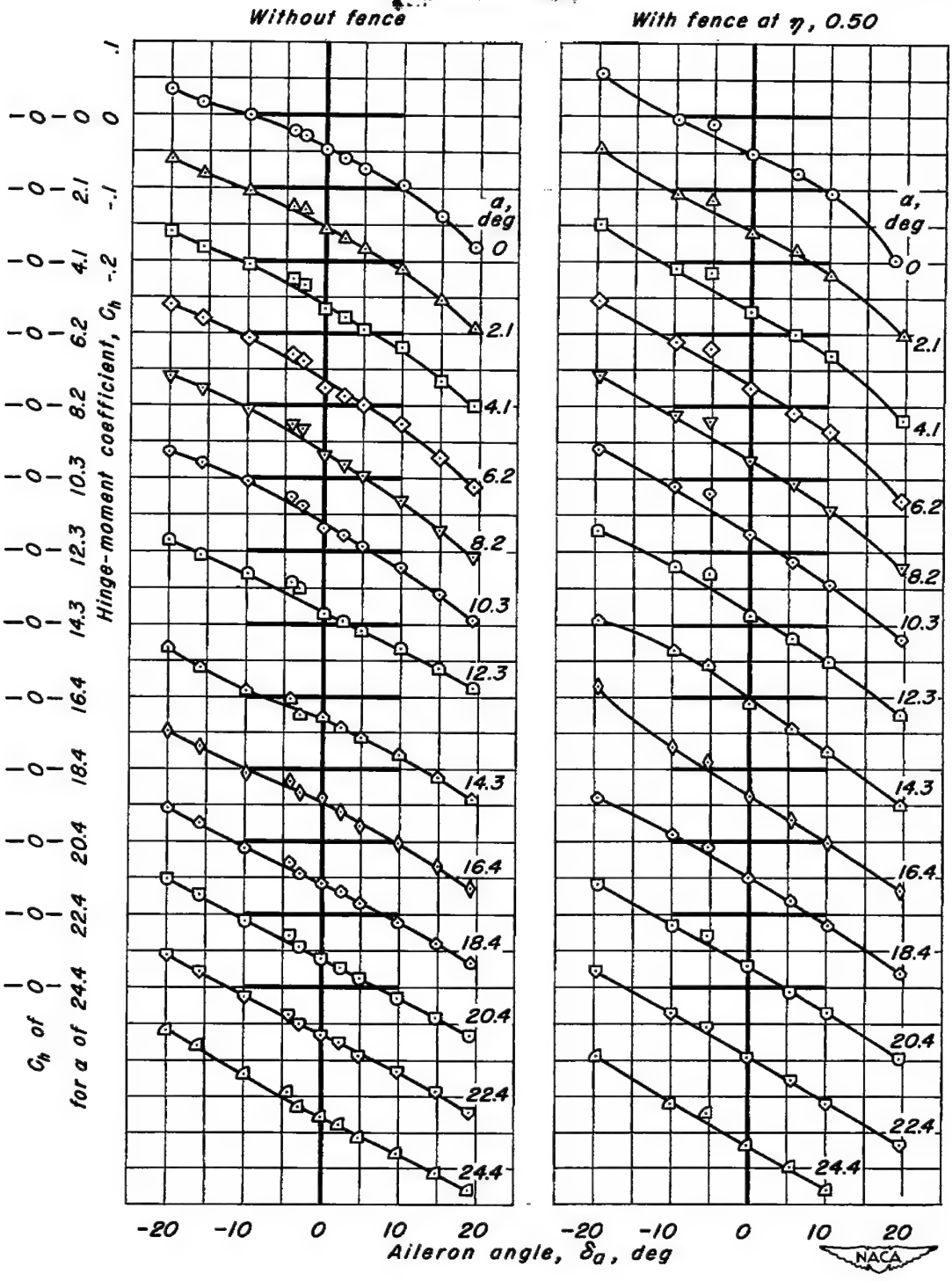

(a) M, 0.25

Figure 10.-The variation of aileron hinge-moment coefficient with aileron angle.

[redacted]

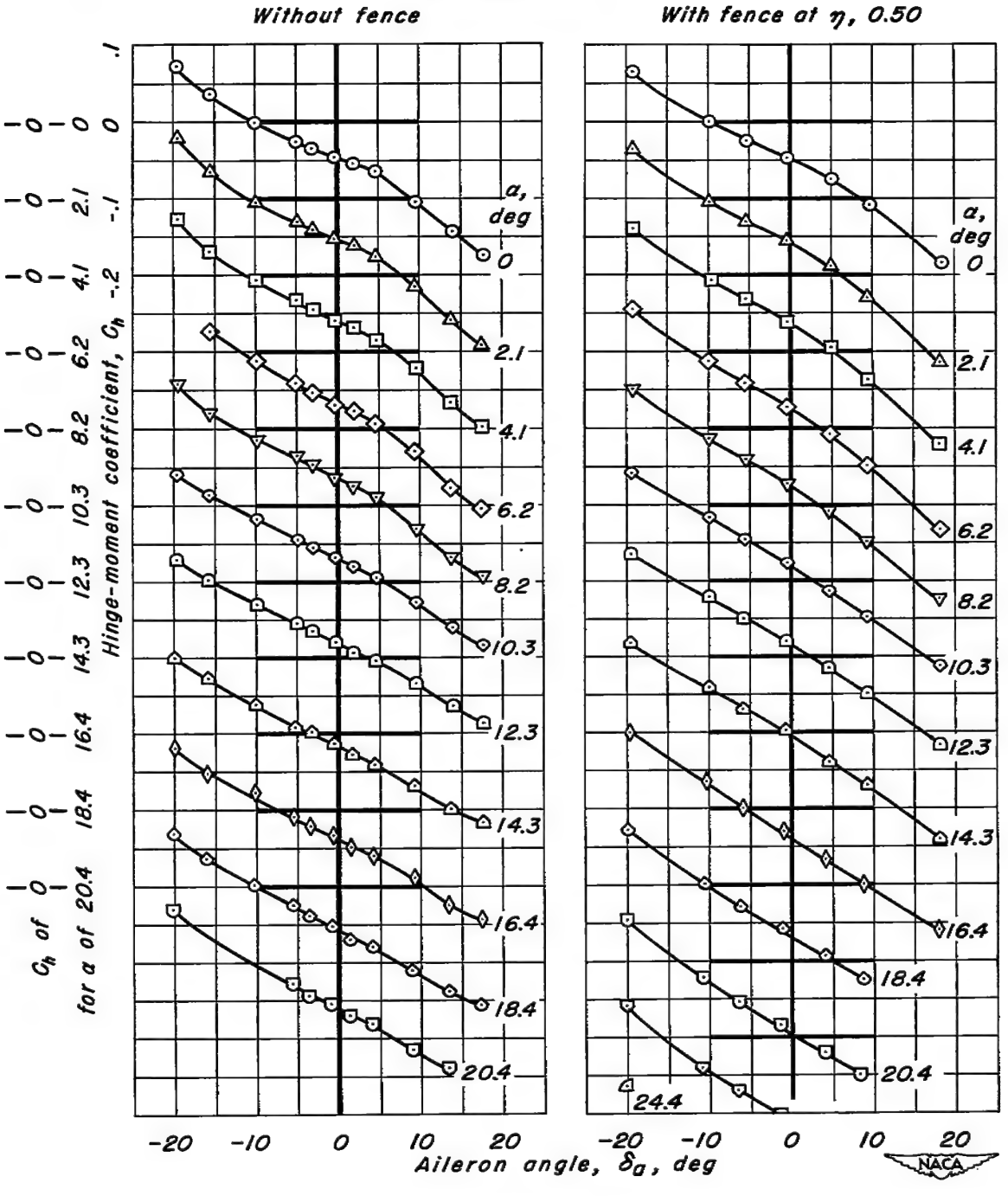

(b) M, 0.80

Figure 10.—Continued.

[redacted]

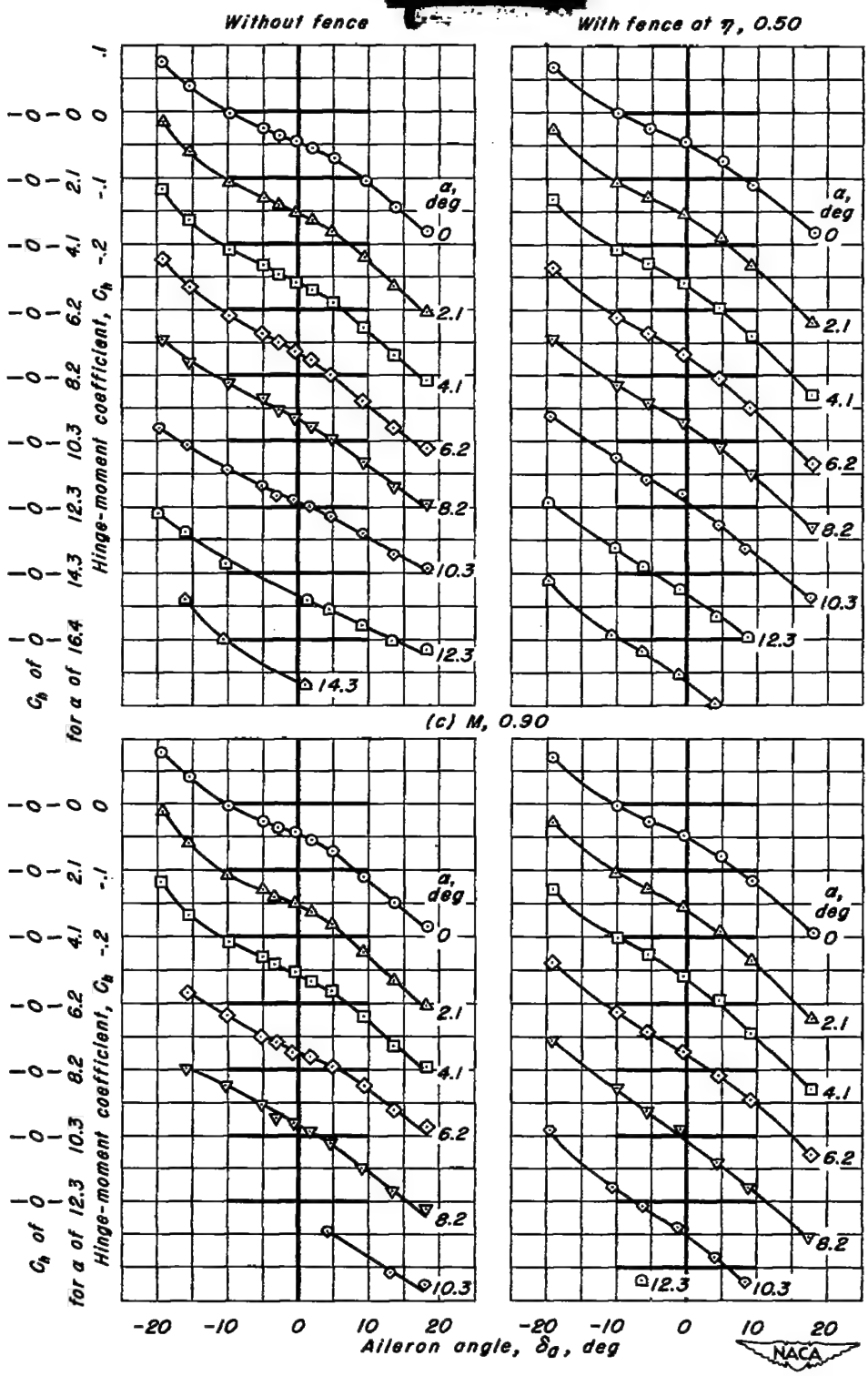

(c) M, 0.90

(d) M, 0.94

Figure 10.—Concluded.

[redacted]

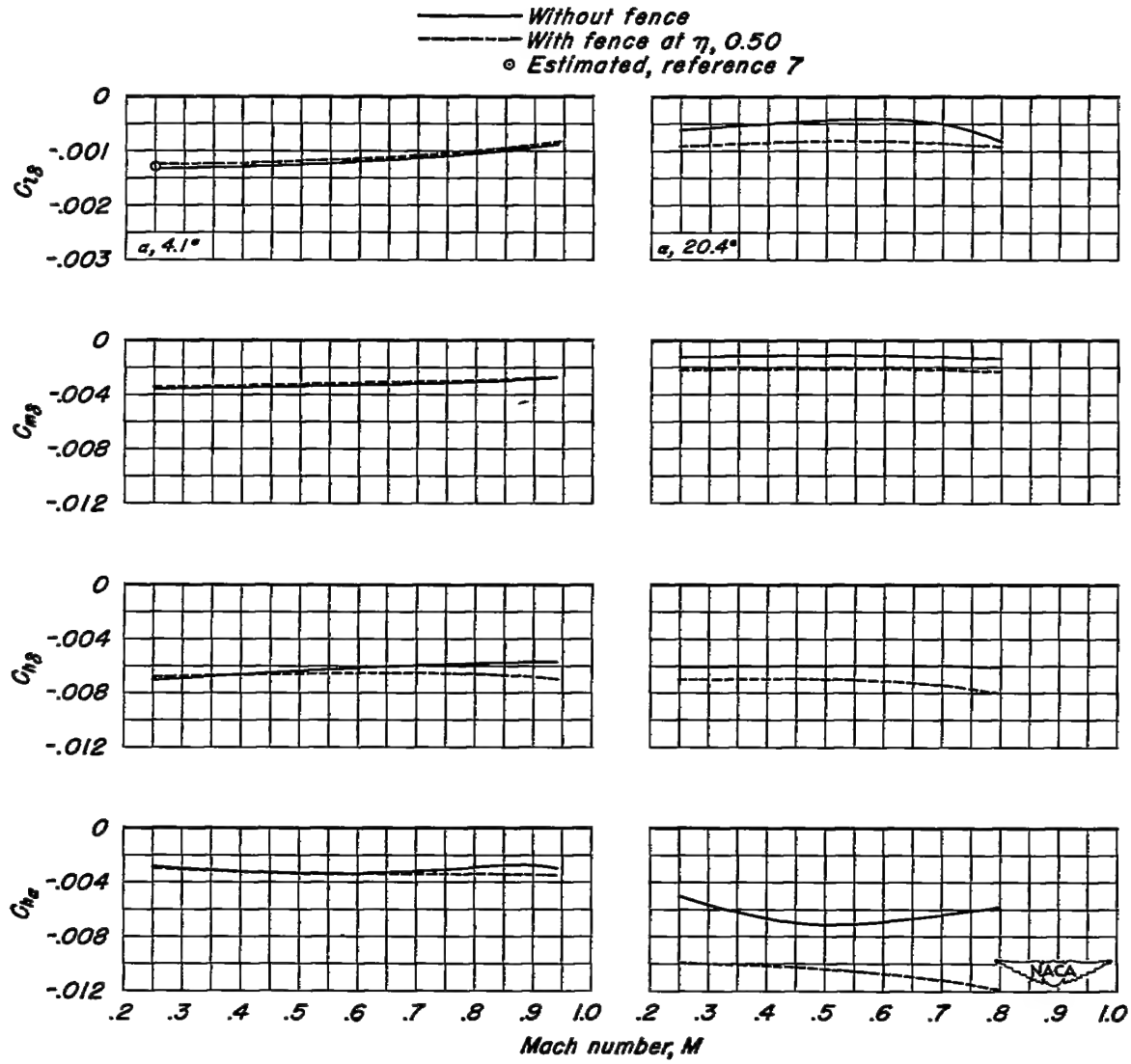

Figure II.- The variation of the aileron effectiveness and hinge-moment parameters with Mach number.

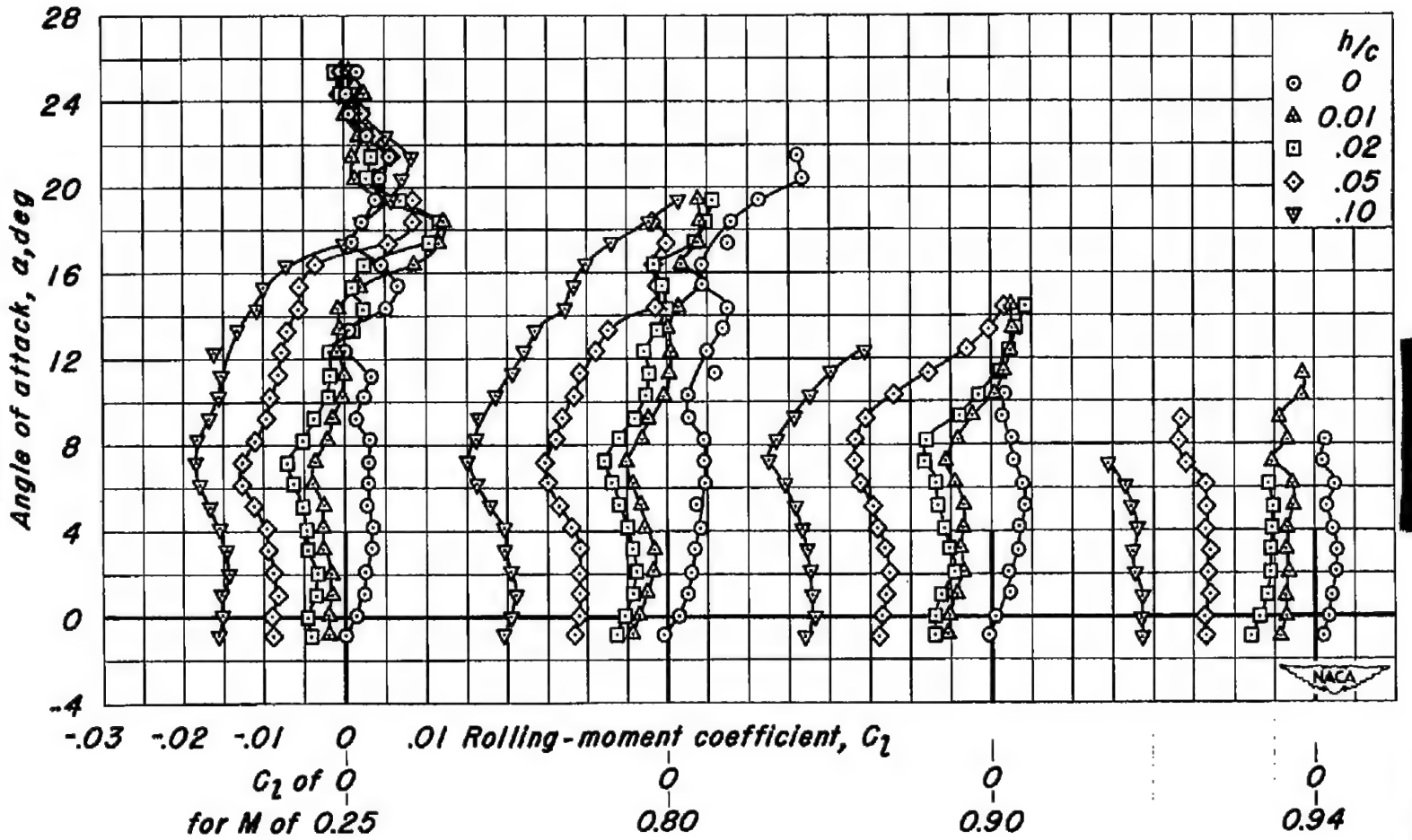

Figure 12.-The rolling-moment characteristics of the continuous spoiler.

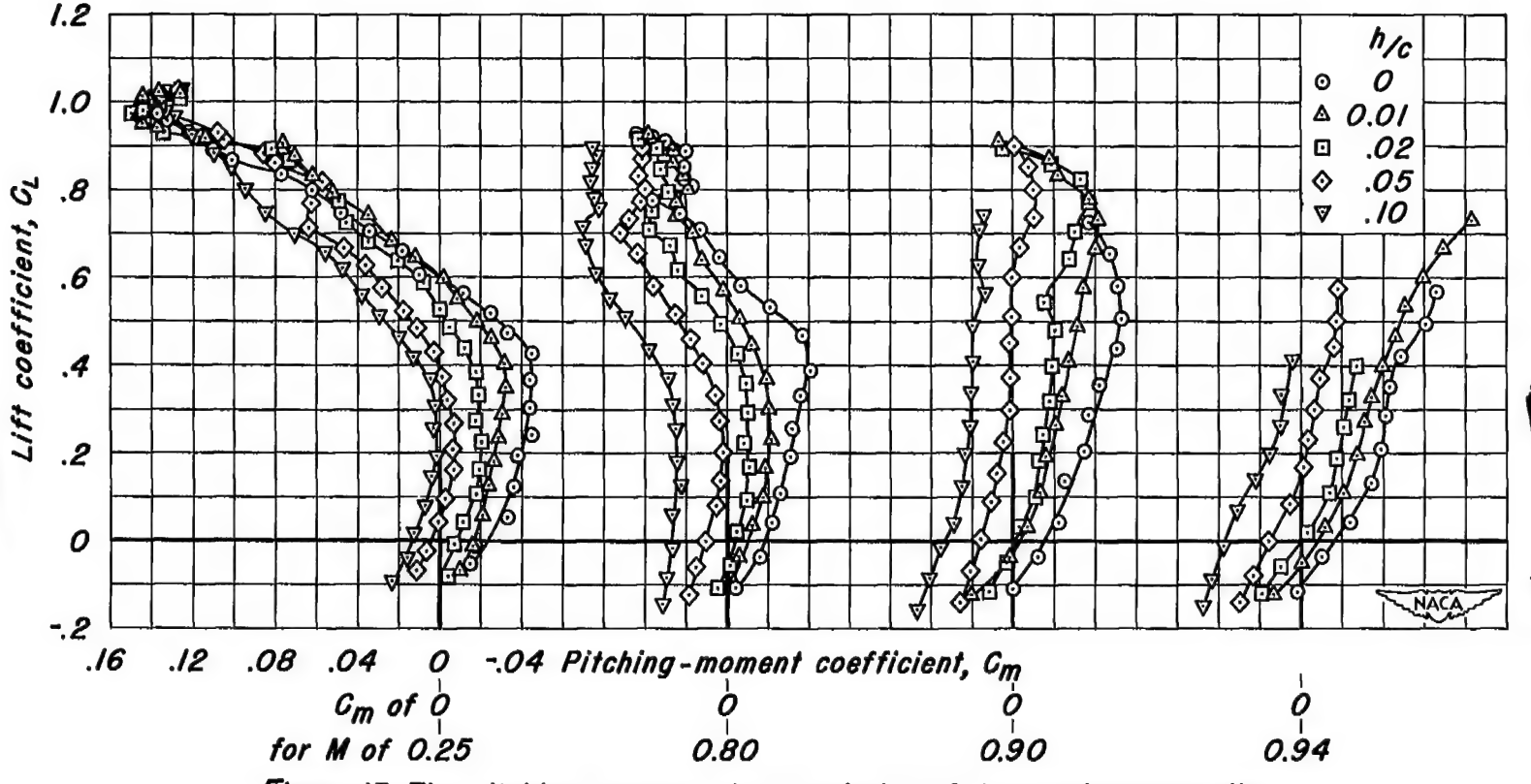

Figure 13.–The pitching-moment characteristics of the continuous spoiler.

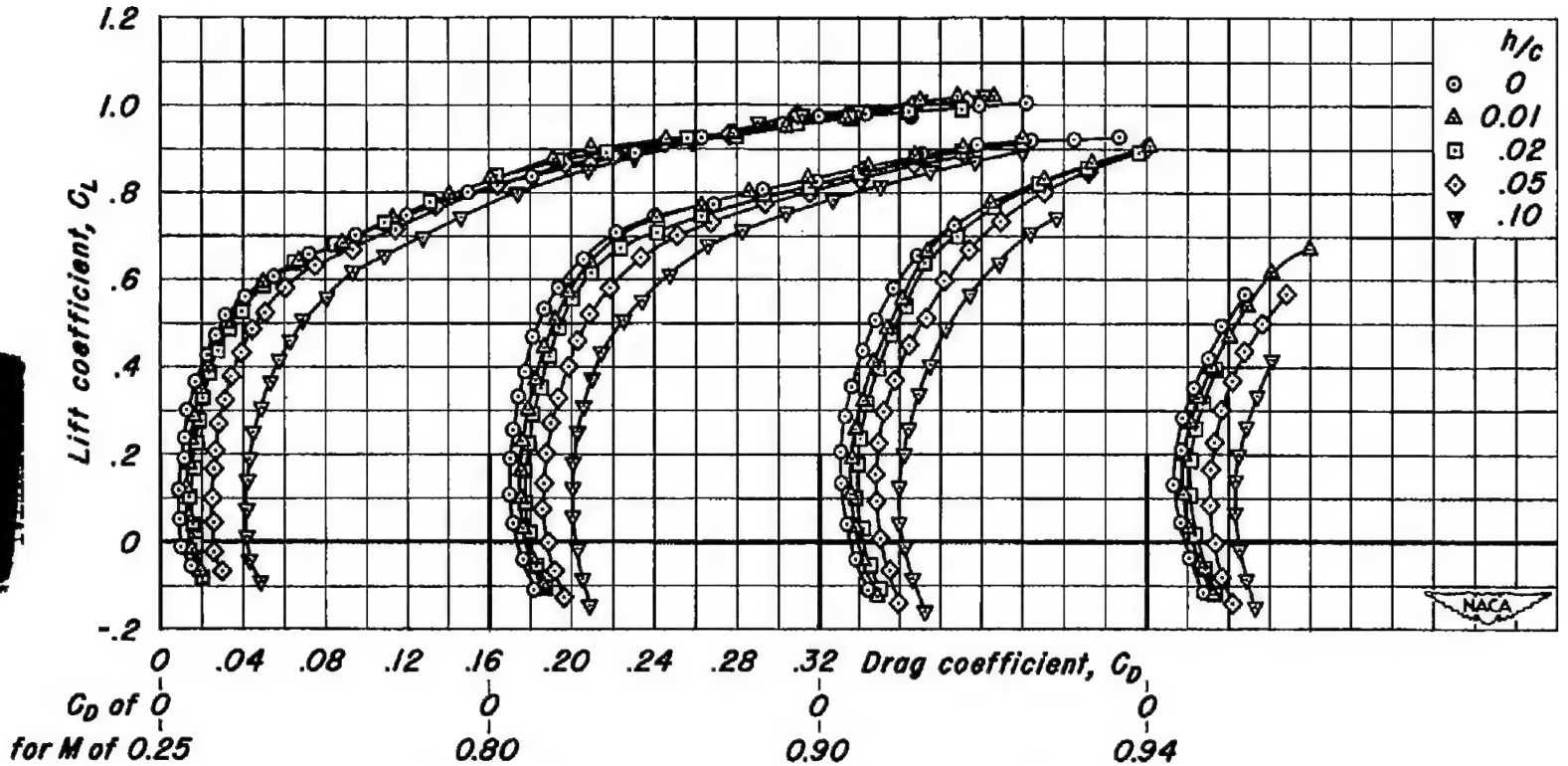

Figure 14.-The drag characteristics of the continuous spoiler.

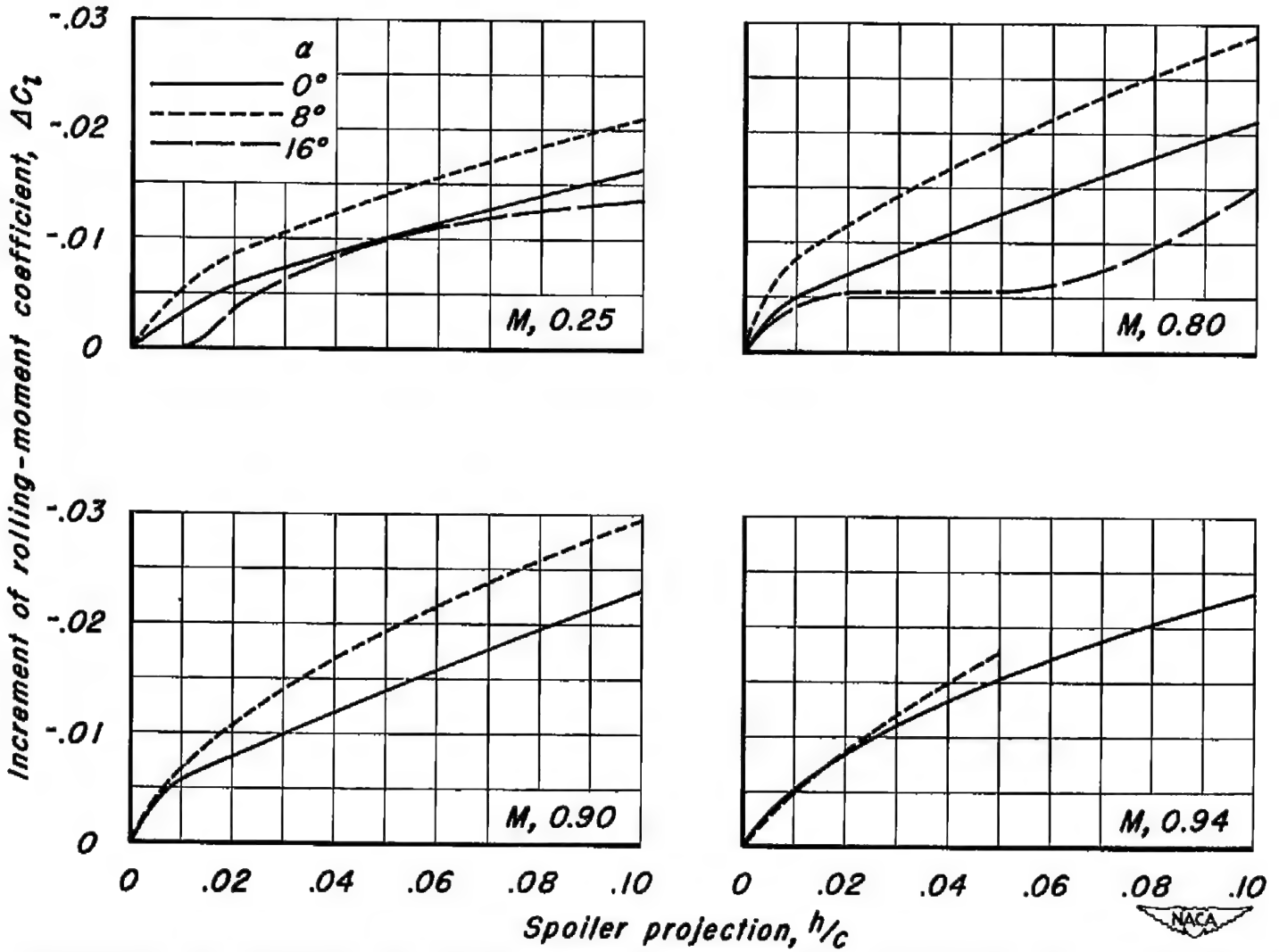

Figure 15.—The variation of incremental rolling-moment coefficient with projection of the continuous spoiler.

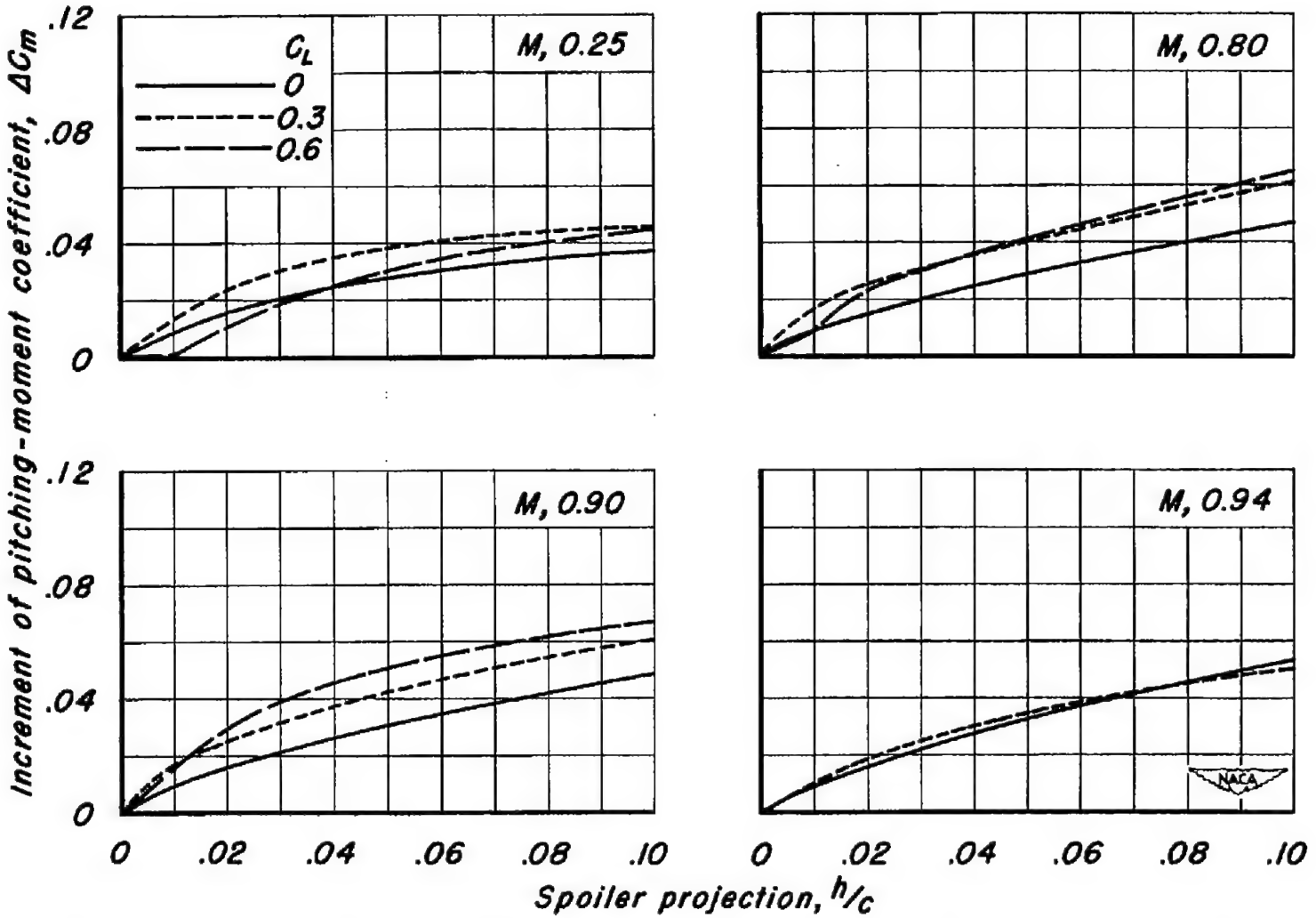

Figure 16.-The variation of incremental pitching-moment coefficient with projection of the continuous spoiler.

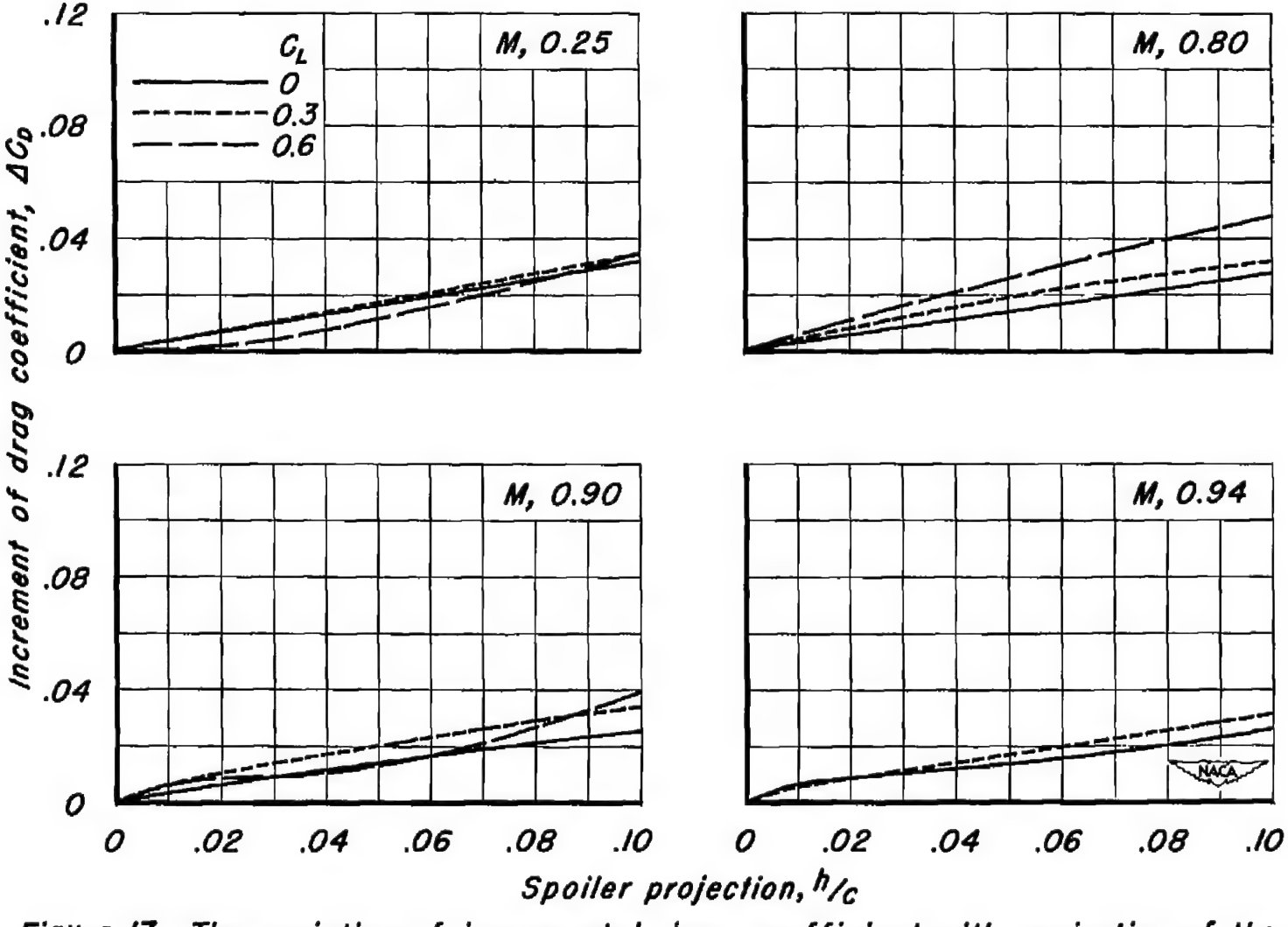

Figure 17.—The variation of incremental drag coefficient with projection of the continuous spoiler.

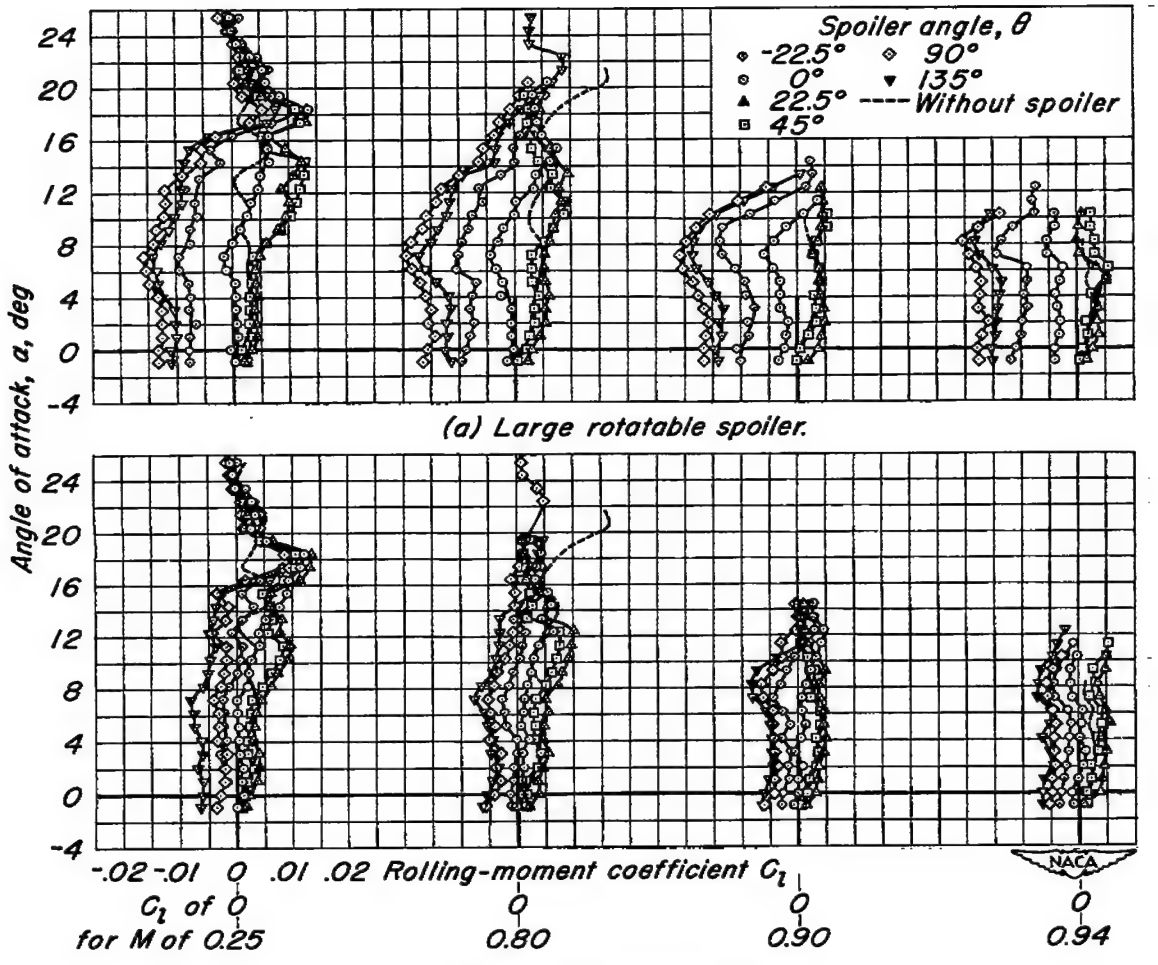

(a) Large rotatable spoiler.

(b) Small rotatable spoiler.

Figure 18.—The rolling-moment characteristics of the rotatable spoilers.

[redacted]

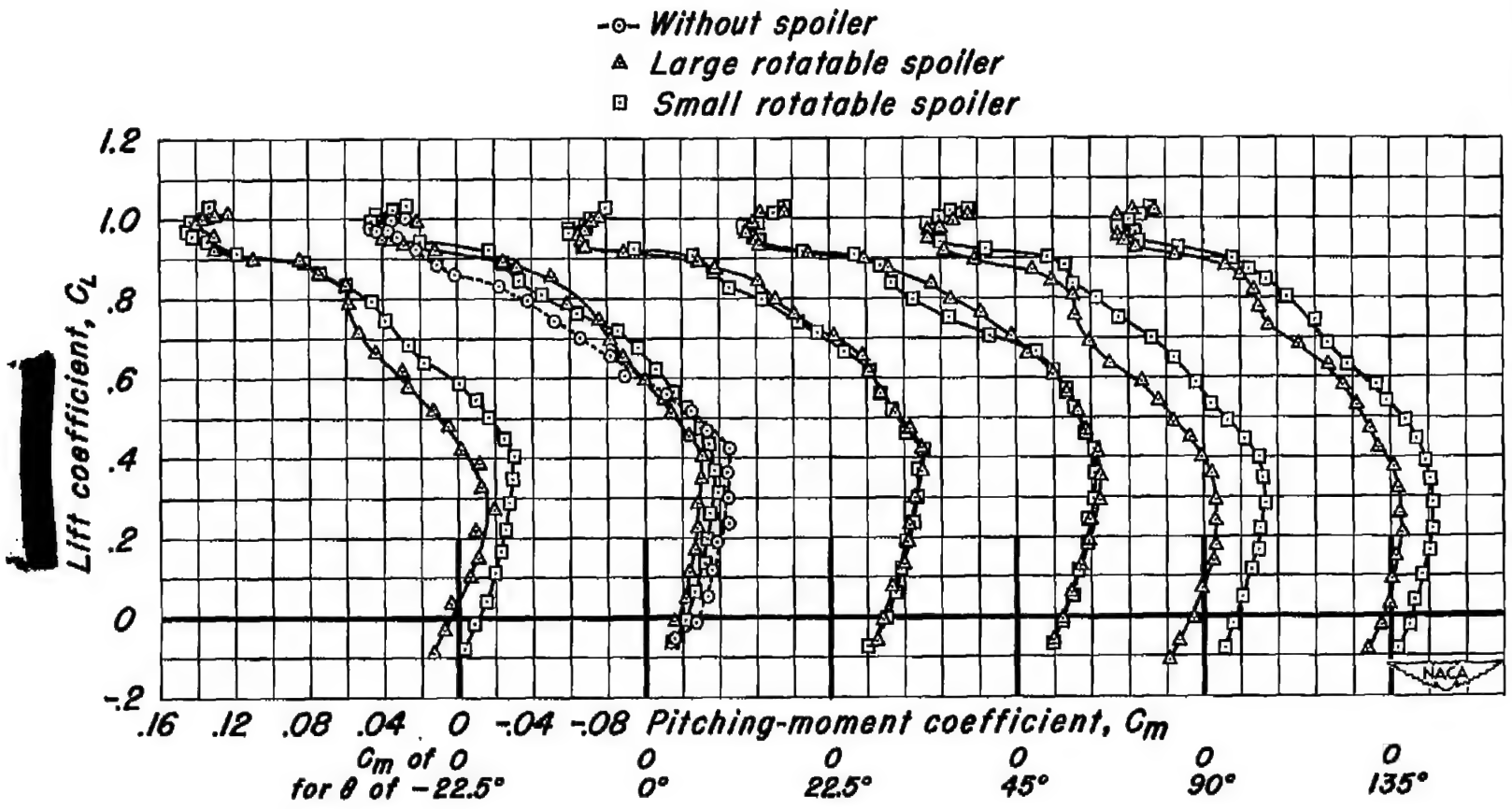

(a) M, 0.25

Figure 19.—The pitching-moment characteristics of the rotatable spoilers.

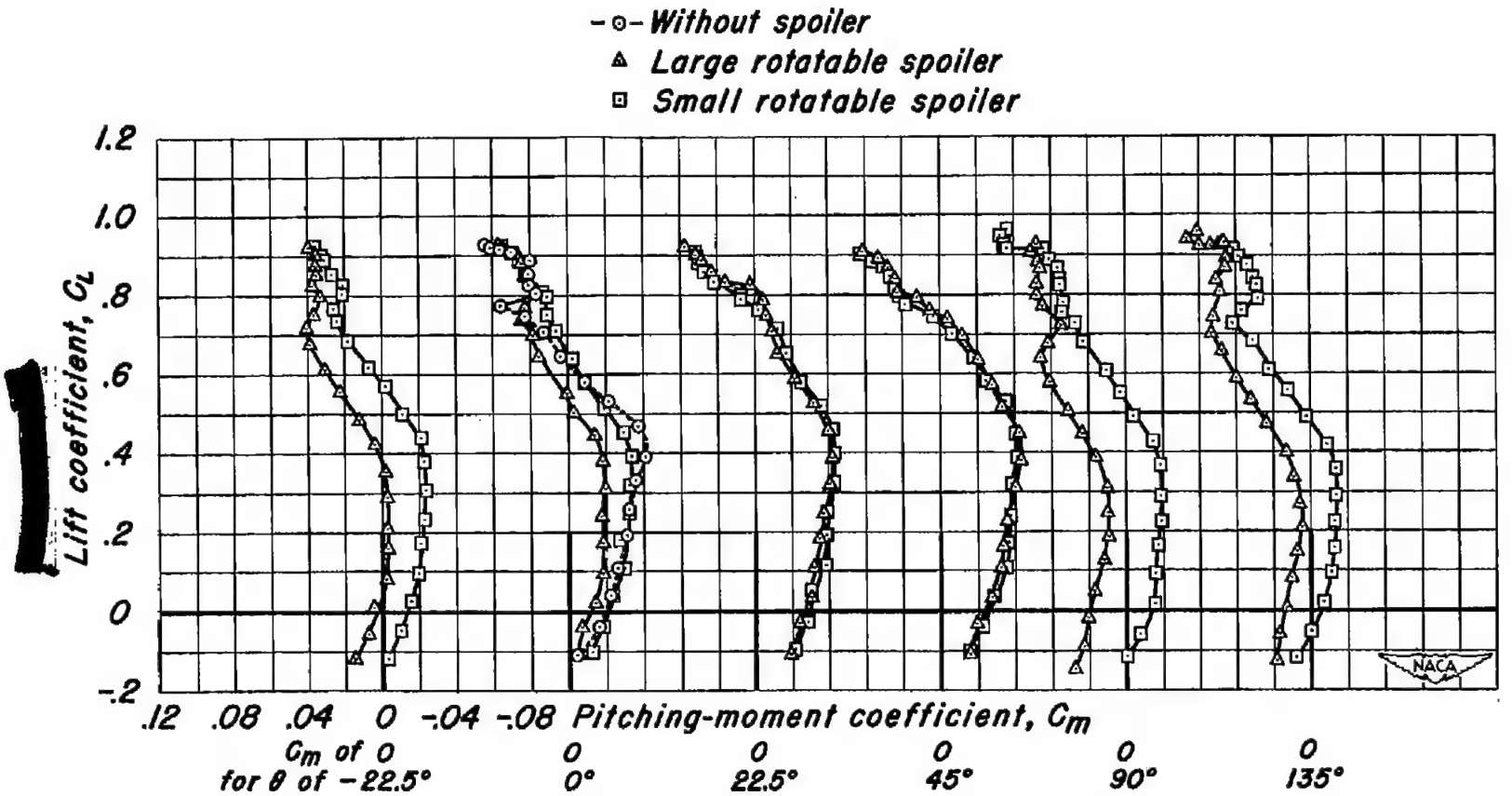

(b) M, 0.80

Figure 19.– Continued.

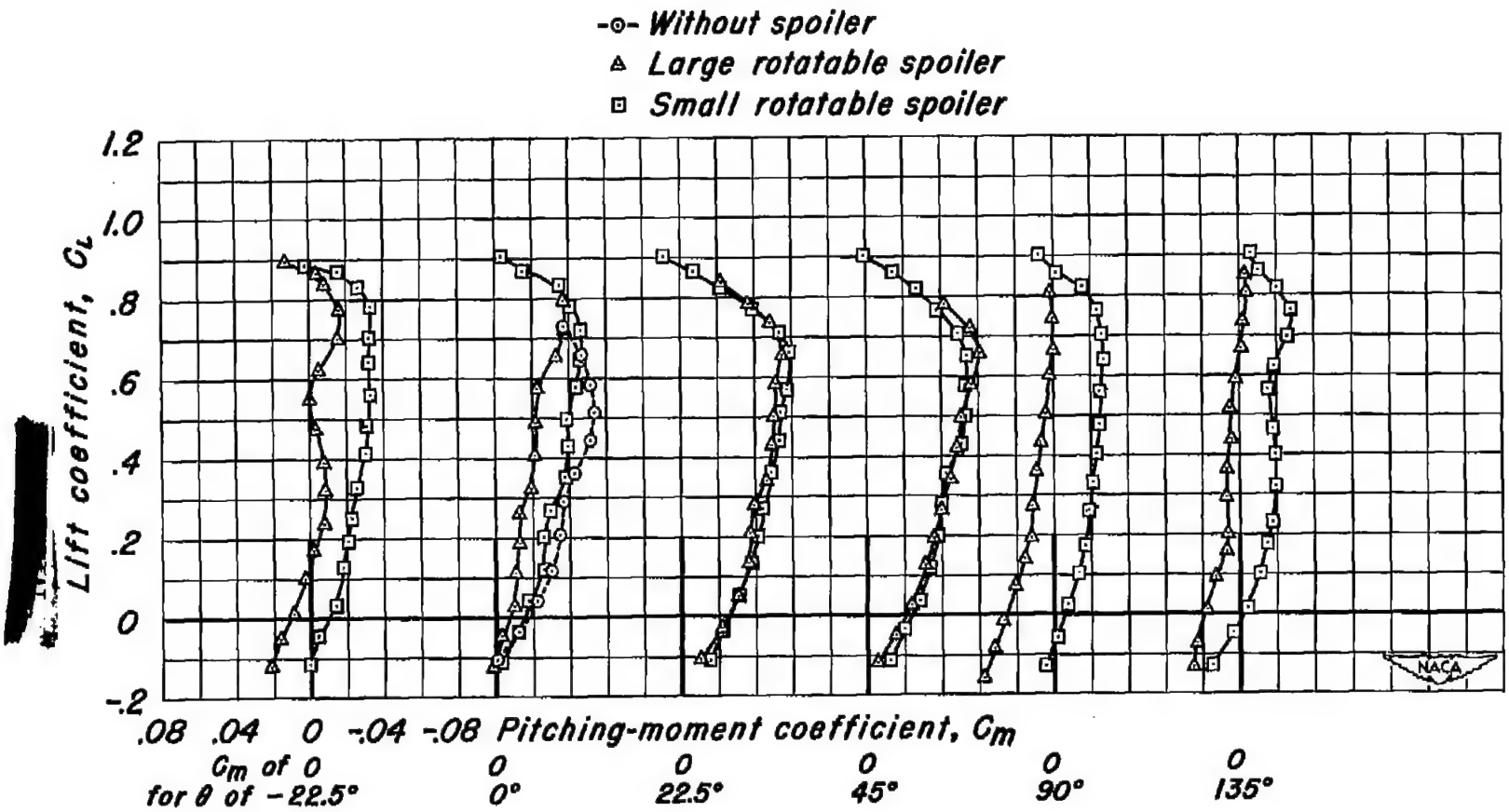

(c) M, 0.90

Figure 19.–Continued.

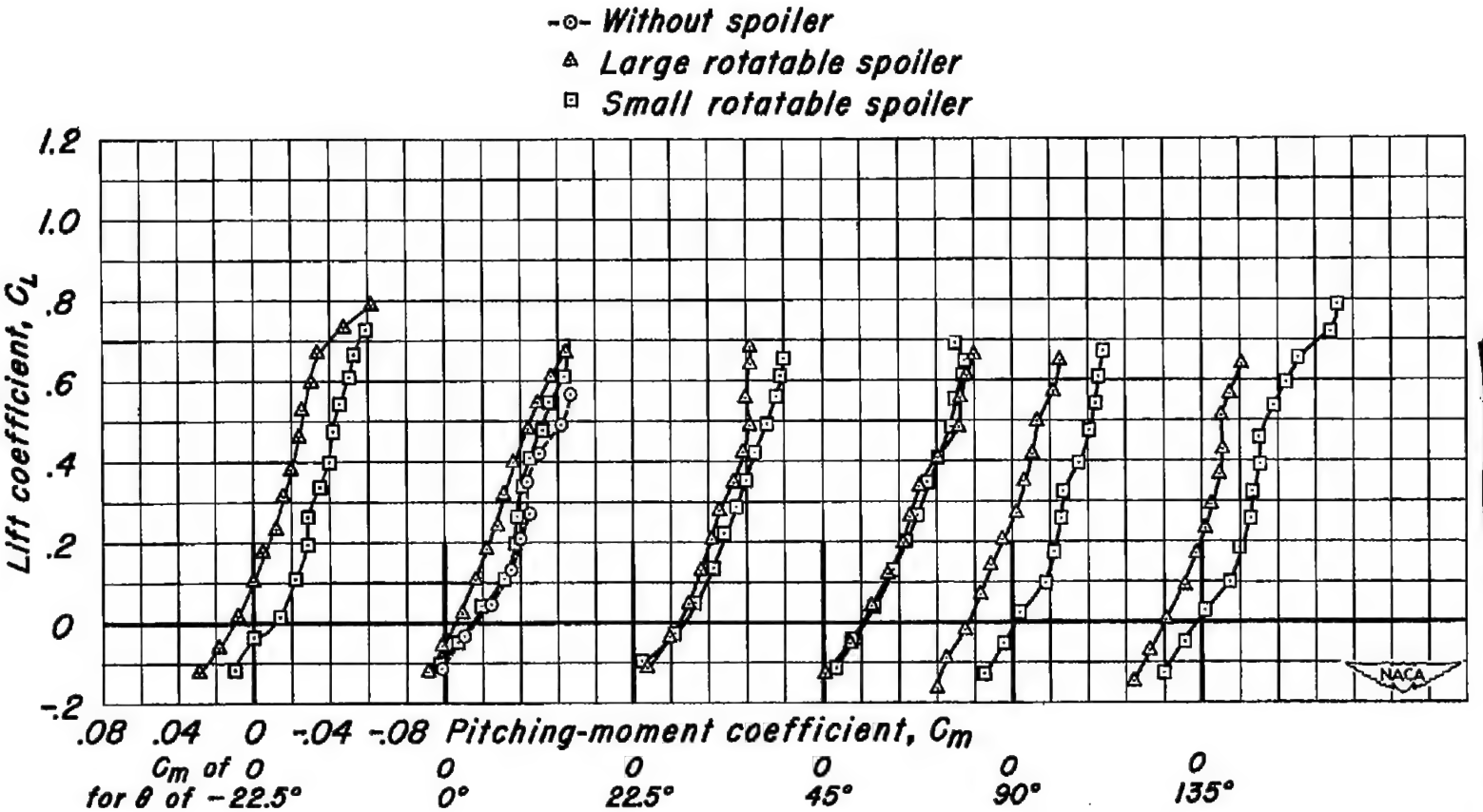

(d) M, 0.94

Figure 19.—Concluded.

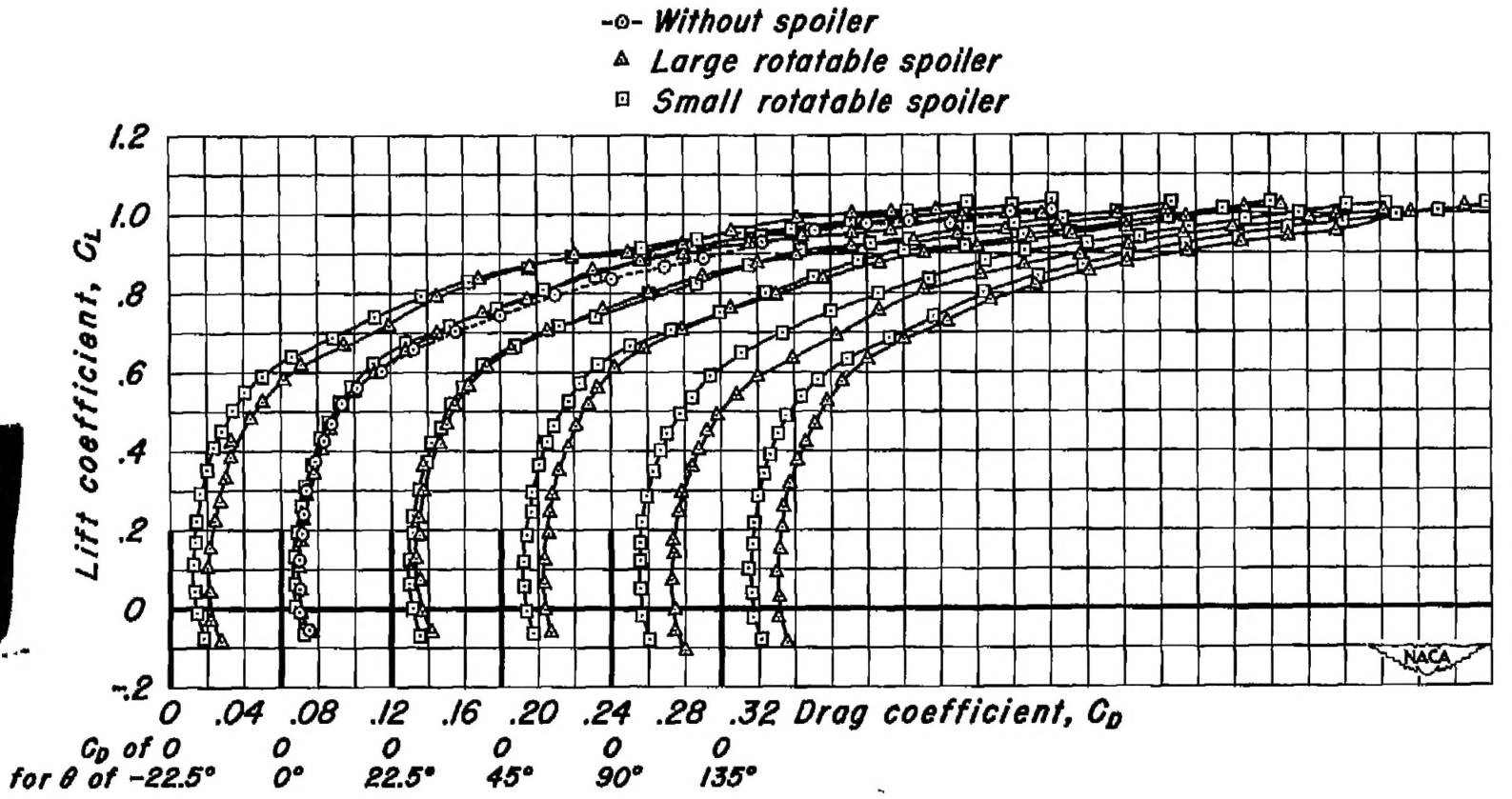

(a) M, 0.25

Figure 20.-The drag characteristics of the rotatable spoiler.

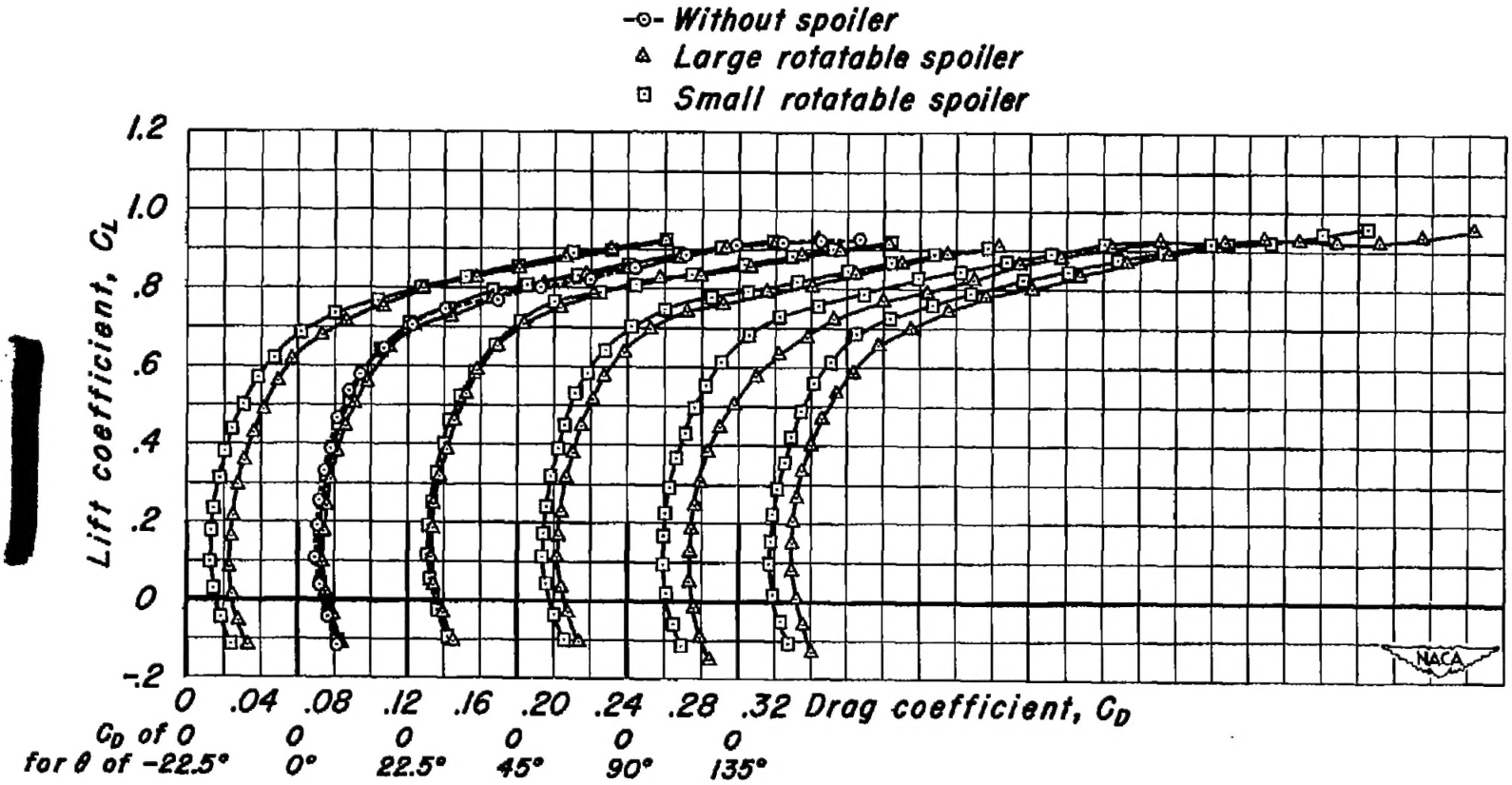

(b) M, 0.80

Figure 20.–Continued.

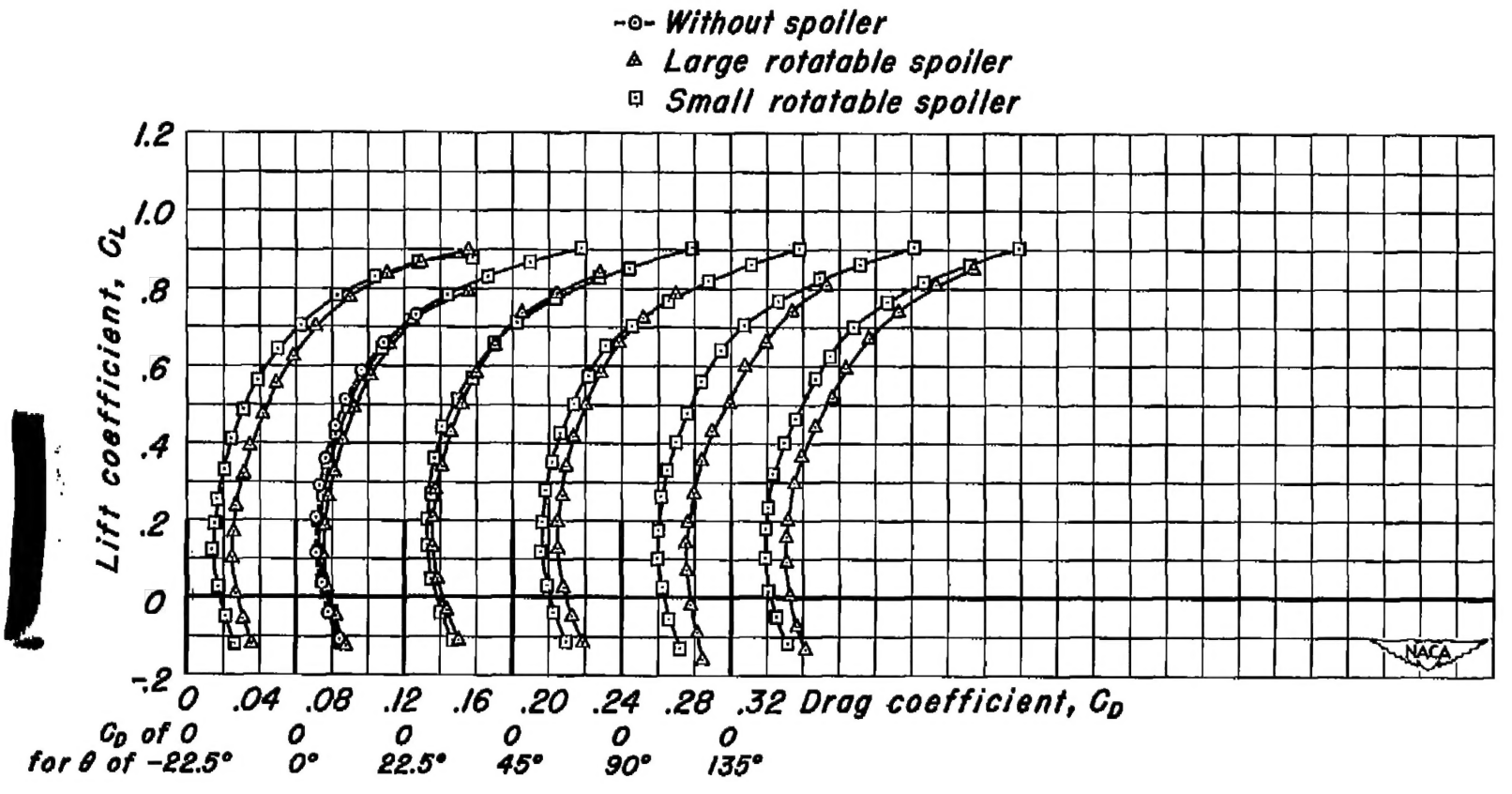

(c) M, 0.90

Figure 20.-Continued.

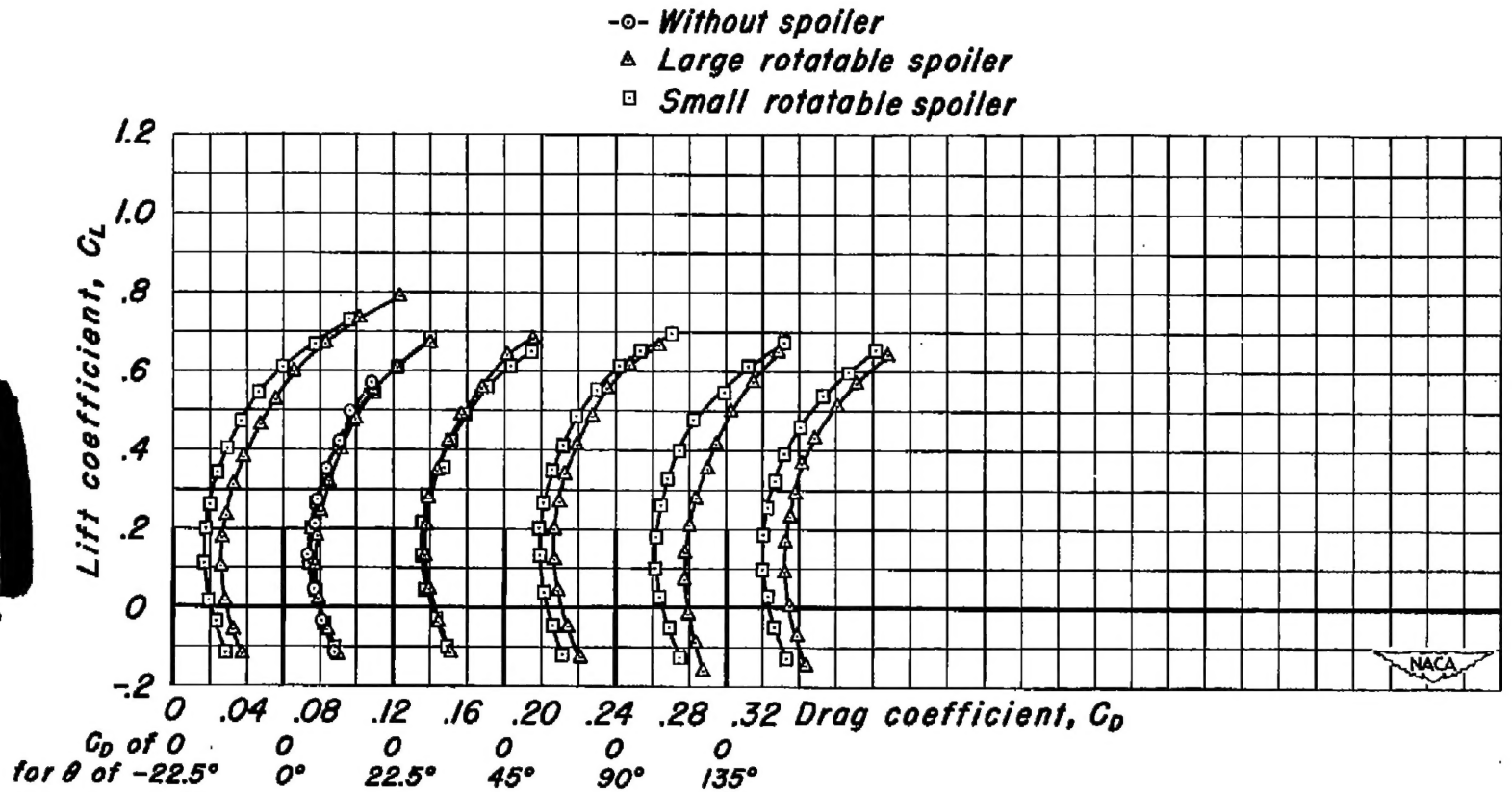

(d) M, 0.94

Figure 20.–Concluded.